PLOS BIOLOGY

RESEARCH ARTICLE

Reservoir host immunology and life history shape virulence evolution in zoonotic viruses

Cara E. Brook[1]*, **Carly Rozins**[2], **Sarah Guth**[3], **Mike Boots**[3,4]

1 Department of Ecology and Evolution, University of Chicago, Chicago, Illinois, United States of America, **2** Department of Science, Technology, and Society, York University, Toronto, Canada, **3** Department of Integrative Biology, University of California, Berkeley, Berkeley, California, United States of America, **4** Biosciences, University of Exeter, Penryn, United Kingdom

* cbrook@uchicago.edu

Citation: Brook CE, Rozins C, Guth S, Boots M (2023) Reservoir host immunology and life history shape virulence evolution in zoonotic viruses. PLoS Biol 21(9): e3002268. https://doi.org/10.1371/journal.pbio.3002268

Academic Editor: James Lloyd-Smith, University of California, Los Angeles, UNITED STATES

Received: September 28, 2022

Accepted: July 21, 2023

Published: September 7, 2023

Data Availability Statement: All relevant data are available within the manuscript and Supporting information files or are deposited in our open access GitHub repository, 'brooklabteam/spillover-virulence: spillover-virulence-v1.0.0' (https://zenodo.org/record/8136864).

Funding: This work was funded by two National Institutes of Health grants (1R01AI129822-01 and 5DP2AI171120-02) to CEB, an Adolph C. and Mary Sprague Miller Institute for Basic Research fellowship to CEB, a Branco Weiss Society in Science fellowship to CEB, an American

Abstract

The management of future pandemic risk requires a better understanding of the mechanisms that determine the virulence of emerging zoonotic viruses. Meta-analyses suggest that the virulence of emerging zoonoses is correlated with but not completely predictable from reservoir host phylogeny, indicating that specific characteristics of reservoir host immunology and life history may drive the evolution of viral traits responsible for cross-species virulence. In particular, bats host viruses that cause higher case fatality rates upon spillover to humans than those derived from any other mammal, a phenomenon that cannot be explained by phylogenetic distance alone. In order to disentangle the fundamental drivers of these patterns, we develop a nested modeling framework that highlights mechanisms that underpin the evolution of viral traits in reservoir hosts that cause virulence following cross-species emergence. We apply this framework to generate virulence predictions for viral zoonoses derived from diverse mammalian reservoirs, recapturing trends in virus-induced human mortality rates reported in the literature. Notably, our work offers a mechanistic hypothesis to explain the extreme virulence of bat-borne zoonoses and, more generally, demonstrates how key differences in reservoir host longevity, viral tolerance, and constitutive immunity impact the evolution of viral traits that cause virulence following spillover to humans. Our theoretical framework offers a series of testable questions and predictions designed to stimulate future work comparing cross-species virulence evolution in zoonotic viruses derived from diverse mammalian hosts.

Introduction

The devastating impact of the Severe Acute Respiratory Syndrome Coronavirus 2 (SARS-CoV-2) pandemic highlights the extreme public health outcomes that can result upon cross-species emergence of zoonotic viruses. Estimating the relative threats posed by potential future zoonoses is an important but challenging public health undertaking. In particular, efforts to predict the virulence of emerging viruses can be complicated since chance will always play a role in dictating the initial spillover that precedes selection [1], virulence upon emergence may be maladaptive in novel hosts [2,3], and patterns in available data may be muddled by

Association for the Advancement of Science/ L'Oréal-USA for Women in Science Fellowship to CEB, and a Defense Advanced Research Projects Agency PREEMPT Program subgrant (D18AC00031) to CEB. This work was further supported by two National Science Foundation-Division of Environmental Biology grants to MB (#2011109 and #2109860). Additionally, CR was supported by the One Health Modelling Network for Emerging Infections (OMNI-RÉUNIS) with the support of Natural Sciences and Engineering Research Council of Canada and the Public Health Agency of Canada. The funders had no role in study design, data collection and analysis, decision to publish, or preparation of the manuscript.

Competing interests: The authors have declared that no competing interests exist.

Abbreviations: BMR, basal metabolic rate; ESS, evolutionarily stable strategy; GAM, generalized additive model; MRCA, most recent common ancestor; SARS-CoV-2, Severe Acute Respiratory Syndrome Coronavirus 2.

attainment bias if avirulent infections go underreported [1]. Nonetheless, a growing body of recent work highlights clear associations between reservoir and spillover host phylogeny and the virulence of a corresponding cross-species infection [4–7]. In many cases, increasing phylogenetic distance between reservoir and spillover hosts is correlated with higher virulence infections [4–6], suggesting that spillover host immune systems may be poorly equipped to tolerate viral traits optimized in more distantly related reservoirs. Still, the effect of phylogeny on spillover virulence appears to supersede that of simple phylogenetic distance [7,8], indicating that taxon-specific reservoir host immunological and life history traits may be important drivers of cross-species virus virulence. Notably, bats host viruses that cause higher human case fatality rates than zoonoses derived from other mammals and birds, a phenomenon that cannot be explained by phylogenetic distance alone [8]. Understanding the mechanisms that select for the evolution of unique viral traits in bats compared to those selected in other mammalian reservoirs should enable us to better predict the virulence of future zoonotic threats.

Although the disproportionate frequency with which the Chiropteran order may source viral zoonoses remains debated [9,10], the extraordinary human pathology induced by many bat-borne zoonoses—including Ebola and Marburg filoviruses, Hendra and Nipah henipaviruses, and SARS, MERS, and SARS-CoV-2 coronaviruses [11]—is not contested. Remarkably, bats demonstrate limited clinical pathology from infection with viruses that cause extreme morbidity and mortality in other hosts [12]. Bats avoid pathological outcomes from viral infection via a combination of unique resistance and tolerance mechanisms, which, respectively, limit the viral load accrued during infection ("resistance") and reduce the disease consequences of a given viral load ("tolerance") [13–16]. Viral resistance mechanisms vary across bat species; those described to date include: receptor incompatibilities that limit the extent of infection for certain viruses in certain bats [17–20], constitutive expression of antiviral cytokines in some bat species [21], and enhanced autophagy [22] and heat-shock protein expression [23] in others. Expansion of anti-viral APOBEC3 genes has also been documented in a few well-studied bat genomes [24,25]. While such robust antiviral immunity would result in widespread immunopathology in most mammals, bats—as the only mammals capable of powered flight—have evolved numerous unique mechanisms of mitigating inflammation incurred during the intensive physiological process of flying [26–28]. These anti-inflammatory adaptations include loss of PYHIN [29–31] and down-regulation of NLRP3 [32] inflammasome-forming gene families, loss of pro-inflammatory genes in the NF-κB pathway [24], dampened interferon activation in the STING pathway [33], and diminished caspase-1 inflammatory signaling [34]. In addition to facilitating flight, this resilience to inflammation has yielded the apparent by-products of extraordinarily long bat lifespans [35] and tolerance of the immunopathology that typically results from viral infection [11]. Moreover, recent work demonstrates how high virus growth rates easily tolerated in constitutively antiviral bat cells cause significant pathology in cells lacking these unique antiviral defenses [36]. The extent to which inflammatory tolerance may modulate the evolution of the viruses that bats host, however, remains largely unexplored.

Modern theory on the evolution of virulence typically assumes, either explicitly or implicitly, that high pathogen growth rates should both enhance between-host transmission and elevate infection-induced morbidity or mortality, resulting in a trade-off between virulence and transmission [37–39]. Theory further suggests that because viral "tolerance" mitigates virulence without reducing viral load, most host strategies of tolerance should select for higher growth rate pathogens that achieve gains in between-host transmission without causing damage to the original host [39–41]. The widely touted viral tolerance of bats [11,16,42–44] should therefore be expected to support the evolution of enhanced virus growth rates, which—though avirulent to bats—may cause significant pathology upon spillover to hosts lacking unique

features of bat immunology and physiology. Beyond tolerance, other life history characteristics unique to diverse reservoir hosts should also impact the evolution of traits in the viruses they host—with important consequences for cross-species virulence following spillover. However, to date, we lack a specific theory that examines the relative impact of reservoir host life history on spillover virulence. Here, we explore the extent to which the immunological and life history traits of mammalian reservoirs can explain variation in the virulence of zoonotic viruses emerging into human hosts.

Results

General trends in the evolution of high growth rate viruses

To elucidate how immunological and life history traits of mammalian hosts combine to drive zoonotic virus virulence, we adopt a nested modeling approach [45], embedding a simple within-host model of viral and leukocyte dynamics within an epidemiological, population-level framework (Fig 1). We examine how the life history traits of a primary reservoir drive the evolution of viral traits likely to cause pathology in a secondary, spillover host—chiefly, a human. Using our nested model in an adaptive dynamics framework [46], we first express the conditions—called the "invasion fitness"—which permit invasion of an evolutionarily "fitter," mutant virus into a reservoir host system in within-host terms. From this, we derive an expression for r_R^*, the optimal within-host growth rate of a persistent virus evolved at equilibrium prevalence in its reservoir host; our modeling framework allows us to express r_R^* as a function of within-host traits that we might expect to vary across mammalian reservoirs with divergent life histories. We deduce that r_R^* can, consequently, also be expected to vary as a result of these life history differences, which modulate the optimization process by which a virus maximizes gains in between-host transmission ($\beta_{r_R}^*$) while mitigating virulence incurred on its reservoir ($\alpha_{r_R}^*$; Fig 1). From this framework, we next derive an expression for α_S, the virulence incurred by a reservoir-optimized virus immediately following spillover to a novel host. We expressed α_S as a function of the reservoir-optimized virus growth rate (r_R^*), combined with spillover host tolerance of virus pathology (T_{vS}), which we model as proportional to the phylogenetic distance between reservoir and spillover host (Fig 1).

Our nested modeling approach first follows Alizon and van Baalen (2005) [45] in derivation of an expression for r_R^*, the within-host virus growth rate optimized based on endemic circulation in a reservoir host. The equation for r_R^* can be captured as follows:

$$r_R^* = \frac{c_R g_{0R}}{m_R} + \frac{\sqrt{c_R^2 m_R^2 g_R g_{0R} \mu_R T_{vR} T_{wR} (v T_{wR} + g_R w T_{vR})}}{m_R^2 (v T_{wR} + g_R w T_{vR})},$$

where μ_R signifies the natural mortality rate of the reservoir host, and all other parameters represent within-host viral and immune dynamics in a persistently infected reservoir. Thus, c_R corresponds to the rate of virus clearance by leukocytes, g_{0R} is the magnitude of constitutive immunity, m_R is the natural leukocyte mortality rate, and g_R is the rate of leukocyte activation following infection, all in the reservoir host. The parameters v and w correspond, respectively, to the intrinsic virulence of the virus and its propensity to elicit a damaging inflammatory response from its host's immune system—while T_{vR} and T_{wR} respectively represent reservoir host tolerance to direct virus pathology and to immunopathology. From the above expression, we explore a range of optimal within-host virus growth rates (r_R^*) for viruses evolved in reservoir hosts with diverse cellular and immunological parameters (Figs 2, S1 and S2 and Table 1). We subsequently calculate the corresponding transmission ($\beta_{r_R}^*$) and virulence ($\alpha_{r_R}^*$) incurred by viruses evolved to r_R^* in their reservoir hosts, then, following Gilchrist and Sasaki (2002)

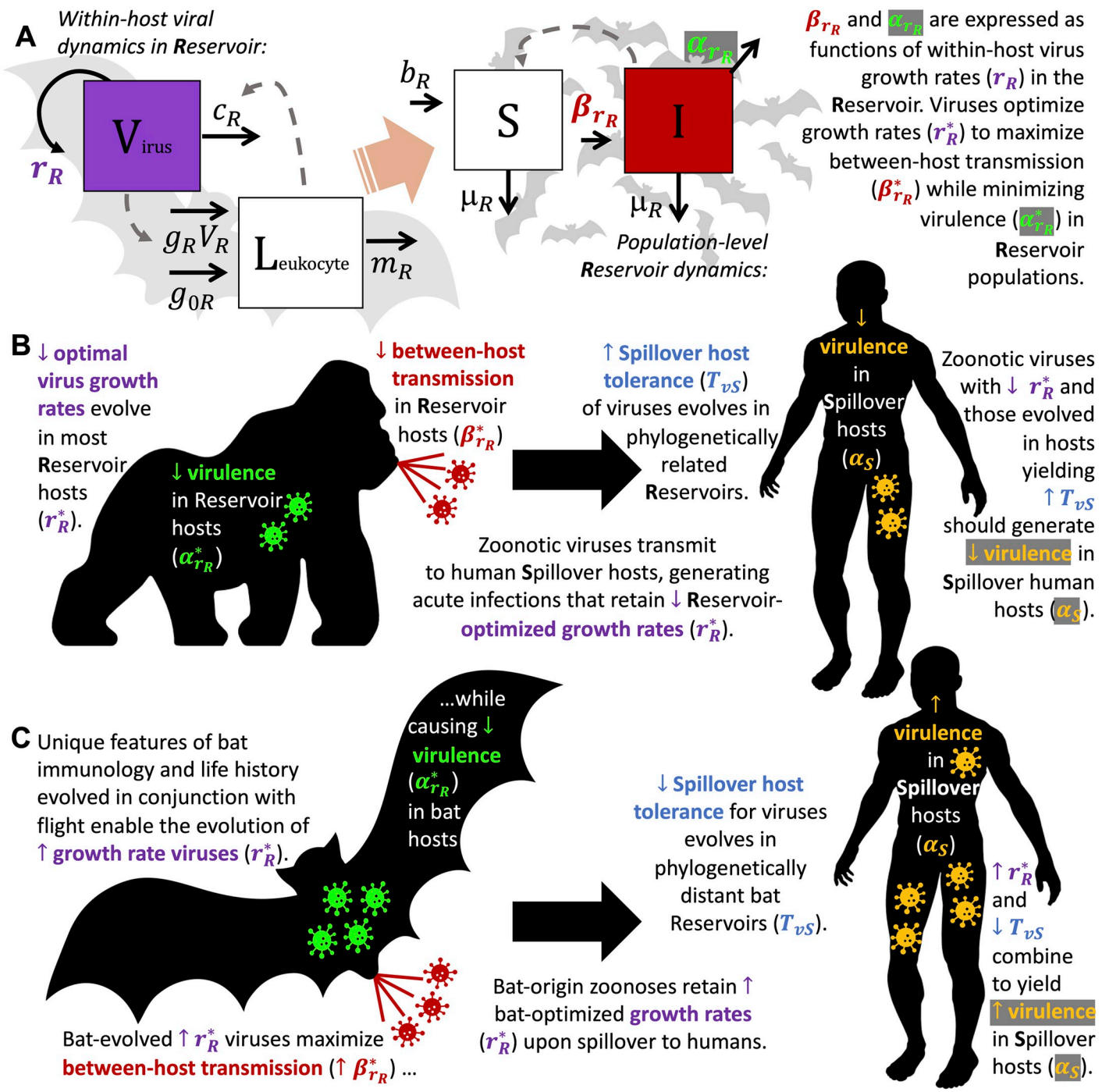

Fig 1. Conceptual mechanistic framework to predict zoonotic virus virulence from reservoir immunology and life history traits. (A) A within-host predator–prey-like model of leukocyte–virus dynamics is embedded in a population-level transmission model for reservoir hosts. Between-host rates of transmission (β_{r_R}) and virulence (α_{r_R}) are expressed as functions of within-host dynamics to derive optimal virus growth rates in the reservoir (r_R^*). See S1 File and Table 1 for parameter definitions and values. (B) Because most mammalian hosts are relatively intolerant of virus pathology and immunopathology, viruses typically evolve low optimal growth rates in reservoir hosts (r_R^*) that minimize virulence incurred on the reservoir ($\alpha_{r_R}^*$). Low growth rates should also generate relatively low between-host transmission in the reservoir population ($\beta_{r_R}^*$). Zoonotic viruses evolved in a reservoir host spillover to human hosts to generate acute infections. These spillover infections yield spillover host virulence (α_S), which we express as a function of the original growth rate of the reservoir-optimized virus (r_R^*), combined with the spillover host tolerance of direct virus pathology (T_{vS}). We model this latter term as inverse to phylogenetic distance between reservoir and spillover (human) host. Zoonoses with low r_R^*—and those from phylogenetically related hosts (like primates) that result in high human T_{vS}—should generate correspondingly low spillover virulence (α_S) in human hosts. (C) As a result of unique bat virus tolerance, viruses evolved in bat reservoir hosts may optimize at high r_R^* values that maximize bat-to-

bat transmission ($\beta^*_{r_R}$) but cause only minimal pathology in the bat host ($\alpha^*_{r_R}$). Such viruses are likely to generate extreme virulence upon spillover (α_S) to secondary hosts, including humans, that lack bat life history traits. The virulence of a virus in its spillover host is amplified (α_S) in cases where large phylogenetic distance between reservoir and spillover host results in minimal spillover host tolerance of virus pathology (T_{vS}).

https://doi.org/10.1371/journal.pbio.3002268.g001

[47], model the nascent spillover of a reservoir-evolved virus as acute infection in a secondary host. In this spillover infection, we assume that the virus retains its reservoir-optimized growth rate (r^*_R) while replicating in the physiological and immunological environment of its novel spillover host. We express this spillover virulence (α_S) as:

$$\alpha_S = V_{S_{avg}}\left(\frac{r^*_R v}{T_{vS}} + \frac{g_S w r^*_R}{T_{wS}}\right),$$

where $V_{S_{avg}}$ corresponds to the average viral load experienced across the timecourse of an acute spillover host infection, and g_S, T_{vS}, and T_{wS} represent the spillover host analogues of previously described within-host parameters in the reservoir host equations (Figs 2, S1, and S2 and Table 1). We present all main text results under assumptions by which tolerance manifests as a constant reduction of either direct virus-induced pathology (T_v) or immunopathology (T_w). See S1 File for comparable results under assumptions of complete tolerance, whereby tolerance completely eliminates virus pathology and immunopathology up to a threshold value, beyond which pathology scales proportionally with virus and immune cell growth.

Our analyses highlight several critical drivers of virus evolution likely to generate significant pathology following spillover to a secondary host (Fig 2): higher within-host virus growth rates (r^*_R) are selected in reservoir hosts with higher background mortality (μ_R), elevated constitutive immune responses (g_{0R}), more rapid leukocyte activation upon infection (g_R), and more rapid virus clearance by the host immune system (c_R). Additionally, higher r^*_R viruses are selected in hosts exhibiting lower leukocyte mortality rates (m_R), resulting in longer-lived immune cells. Critically, higher reservoir host tolerance of both virus-induced pathology (T_{vR}) and immunopathology (T_{wR}) also select for higher r^*_R. In keeping with trade-off theory, changes in the majority of within-host parameters drive corresponding increases in r^*_R, $\beta^*_{r_R}$, and $\alpha^*_{r_R}$, such that viruses evolved to high growth rates experience high transmission within the reservoir host population—but also generate high virus-induced mortality (Fig 2). By definition, the 2 modeled mechanisms of tolerance (T_{vR} and T_{wR}) decouple the relationship between transmission and virulence, permitting evolution of high r^*_R viruses that achieve gains in between-host transmission ($\beta^*_{r_R}$), while simultaneously incurring minimal virulence ($\alpha^*_{r_R}$) on reservoir hosts. By extension, we demonstrate that viruses evolving high optimal r^*_R values in reservoir hosts incur substantial pathology upon spillover to secondary hosts (α_S). Intriguingly, the virulence that a virus incurs on its spillover host (α_S) accelerates substantially faster than that incurred on its reservoir host ($\alpha^*_{r_R}$) at higher values for certain parameters, chiefly, g_{0R}, c_R as well as, most critically, T_{vR} and T_{wR}. This underscores the important capacity of these within-host traits to drive cross-species virulence in emerging viruses.

Order-specific estimates for optimal virus growth rates evolved in reservoir hosts

We next apply our model to attempt to make broad predictions of the evolution of optimal virus growth rates (r^*_R) across diverse mammalian reservoir orders, based on order-specific variation in 3 key parameters from our nested model: the reservoir host background mortality

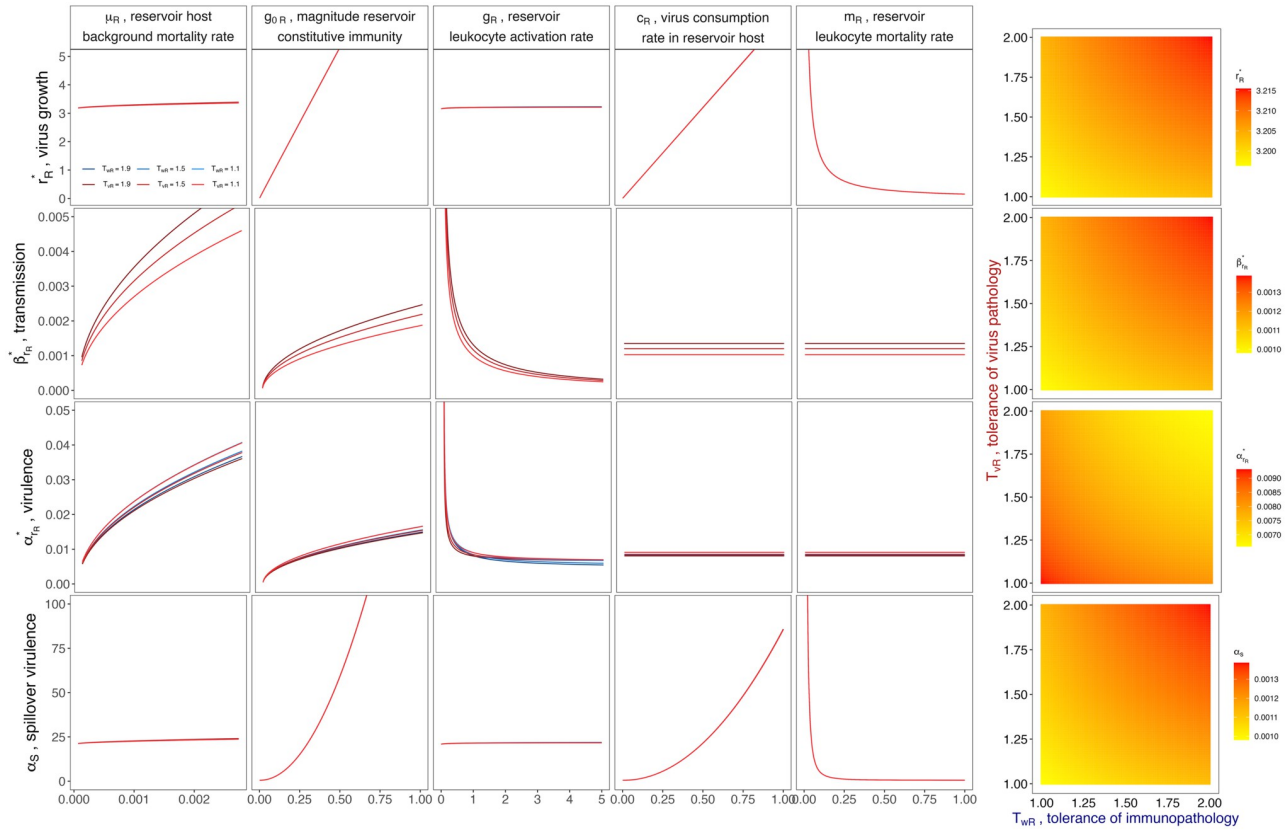

Fig 2. Optimal virus growth rates—and subsequent spillover virulence—vary across reservoir host immunological and life history parameters. Rows (top-down) indicate the evolutionarily optimal within-host virus growth rate (r_R^*) and the corresponding between-host transmission rate ($\beta_{r_R}^*$), and virus-induced mortality rate ($\alpha_{r_R}^*$) for a reservoir host infected with a virus at r_R^*. The bottom row then demonstrates the resulting virulence (α_S) of a reservoir-optimized virus evolved to r_R^* upon nascent spillover to a novel, secondary host. Columns demonstrate the dependency of these outcomes on variable within-host parameters in the reservoir host: background mortality (μ_R), magnitude of constitutive immunity (g_{0R}), rate of leukocyte activation upon viral contact (g_R), rate of virus consumption by leukocytes (c_R), and leukocyte mortality rate (m_R). Darker colored lines depict outcomes at higher reservoir host tolerance of direct virus pathology (T_{vR}, red) or immunopathology (T_{wR}, blue), assuming no tolerance of the opposing type. Heat maps demonstrate how T_{vR} and T_{wR} interact to produce each outcome. Parameter values are reported in Table 1. Figure assumes tolerance in the "constant" form. See S2 Fig for "complete" tolerance assumptions and S3 Fig for changes in α_S across a variable range of parameter values for spillover host tolerance of direct virus pathology, T_{vS}, and immunopathology, T_{wS}. Data and code used to generate all figure panels are available in our publicly available GitHub repository (github.com/brooklabteam/spillover-virulence-v1.0.0; doi: 10.5281/zenodo.8136864).

https://doi.org/10.1371/journal.pbio.3002268.g002

rate (μ_R), the reservoir host tolerance of immunopathology (T_{wR}), and the reservoir host magnitude of constitutive immunity (g_{0R}). Within-host immunological data needed to quantify these parameters is lacking for most taxa; thus, we use regression analyses to summarize these terms across mammalian orders from publicly available life history data. In particular, we use well-described allometric relationships between mammalian body mass and basal metabolic rate (BMR) with lifespan and immune cell concentrations [49–53] to proxy μ_R, T_{wR}, and g_{0R} across mammalian orders (Figs 3A–C, S4 and S1 Table). From here, we use our nested modeling framework to predict optimal virus growth rates (r_R^*) across diverse mammalian reservoirs (Fig 3D). Then, we estimate T_{vS}, the spillover host tolerance of direct virus pathology, as proportional to the time to most recent common ancestor (MRCA) between the human primate order and each mammalian reservoir order, now focusing our analysis on zoonotic spillover (Fig 3E and 3F and S1 Table). Finally, we combine estimates for r_R^* and T_{vS} to generate a prediction for α_S, the virulence of a reservoir-optimized virus in a human spillover host, which we

Table 1. Default parameter values for population-level and within-host models.

Parameter	Definition	Units	Value*	Scale
b_R	reservoir host natural birth rate	$days^{-1}$	0.2	population-level
q_R	reservoir host crowding term to regulate density-dependent growth	$days^{-1}$	0.002	population-level
$\mu_R^{\dagger}$	reservoir host background mortality rate	$days^{-1}$	$\frac{1}{20*365}$	population-level
$g_{0R}^{\dagger}$	reservoir host magnitude of constitutive immunity *(rate of baseline neutrophil supply)*	$days^{-1}$	.3	within-host
g_R	rate of leukocyte activation by virus	$days^{-1}$	0.9	within-host
c_R	rate of virus consumption by leukocyte	$days^{-1}$	0.5	within-host
m_R	background mortality rate for leukocytes	$days^{-1}$	$\frac{1}{21}$	within-host
ζ	scaling factor translating within-host viral load to between-host transmission rate	$days^{-1}$	0.2	within-host
w	intrinsic virus propensity to elicit inflammatory immune response from host	$leukocytes^{-1}$	1	within-host
v	intrinsic virus virulence	$virions^{-1}$	1	within-host
$T_{wR}{}^{\dagger}$	reservoir host tolerance of immunopathology (constant or complete)	unitless	*variable* constant: 1 – 2 complete: 0 – 1	within-host
T_{vR}	reservoir host tolerance of virus pathology (constant or complete)	unitless	*variable* constant: 1 – 2 complete: 0 – 1	within-host
$T_{vS}{}^{\dagger}$	human tolerance of viral pathology (constant or complete)	unitless	*variable* constant: 1 – 2 complete: 0 – 1	between-host spillover

*Value column gives parameter values fixed in Figs 2 and S2, excepting instances when parameter was modulated along the x-axis or internally (T_{wR}, T_{vR}) as indicated in the figure legend. Parameter values are comparable to the ranges explored in Miller and colleagues [40] and Boots and colleagues [48].

†Parameters μ_R, g_{0R}, T_{wR}, and T_{vS} were modeled as functions of mammalian order-specific life history traits in Figs 3 and S4–S9, as outlined in the Methods.

https://doi.org/10.1371/journal.pbio.3002268.t001

can compare against case fatality rates for mammalian zoonoses reported in the literature [4,8] (Figs 3G and S5–S9).

We first fit a simple linear regression to the response variable of the inverse of maximum lifespan across diverse mammalian hosts with a single predictor of reservoir host order (Fig 3A and S2 Table). From this simple model, we can easily make projections that summarize μ_R, the reservoir host annual mortality rate, to an average value for each of 26 mammalian orders. We express μ_R in units of $days^{-1}$ on a timescale most relevant to viral dynamics; as a result, even multiyear differences in maximum longevity do little to drive differences in μ_R across mammalian orders. Nonetheless, 8 orders (Afrosoricida, Dasyuromorphia, Didelphimorphia, Eulipotyphla, Macroscelidea, Notoryctemorphia, Peramelemorphia, and Rodentia) demonstrate significantly elevated annual mortality rates using the median order mortality rate (Diprotodontia) as a reference. By contrast, Carnivora, Cetartiodactyla, Primates, and Perissodactyla demonstrate significantly reduced annual mortality rates as compared to the same reference (Fig 3C and S1 and S2 Tables).

Drawing on well-described allometric relationships between mass and lifespan [49] and more recent literature that links longevity with resilience to inflammation [11,44,57–61], we next sought to characterize variation in T_{wR}, reservoir host tolerance of immunopathology, across mammalian orders. Smaller-bodied organisms are hypothesized to be shorter-lived due to higher metabolic rates, more rapid energy expenditure, and faster accumulation of oxidative damage, which can manifest as inflammation [62]. We hypothesized, then, that organisms that are longer-lived than predicted for their body size might be more resilient to inflammatory stressors—and, therefore, by extension, more tolerant of immunopathology. Building on this

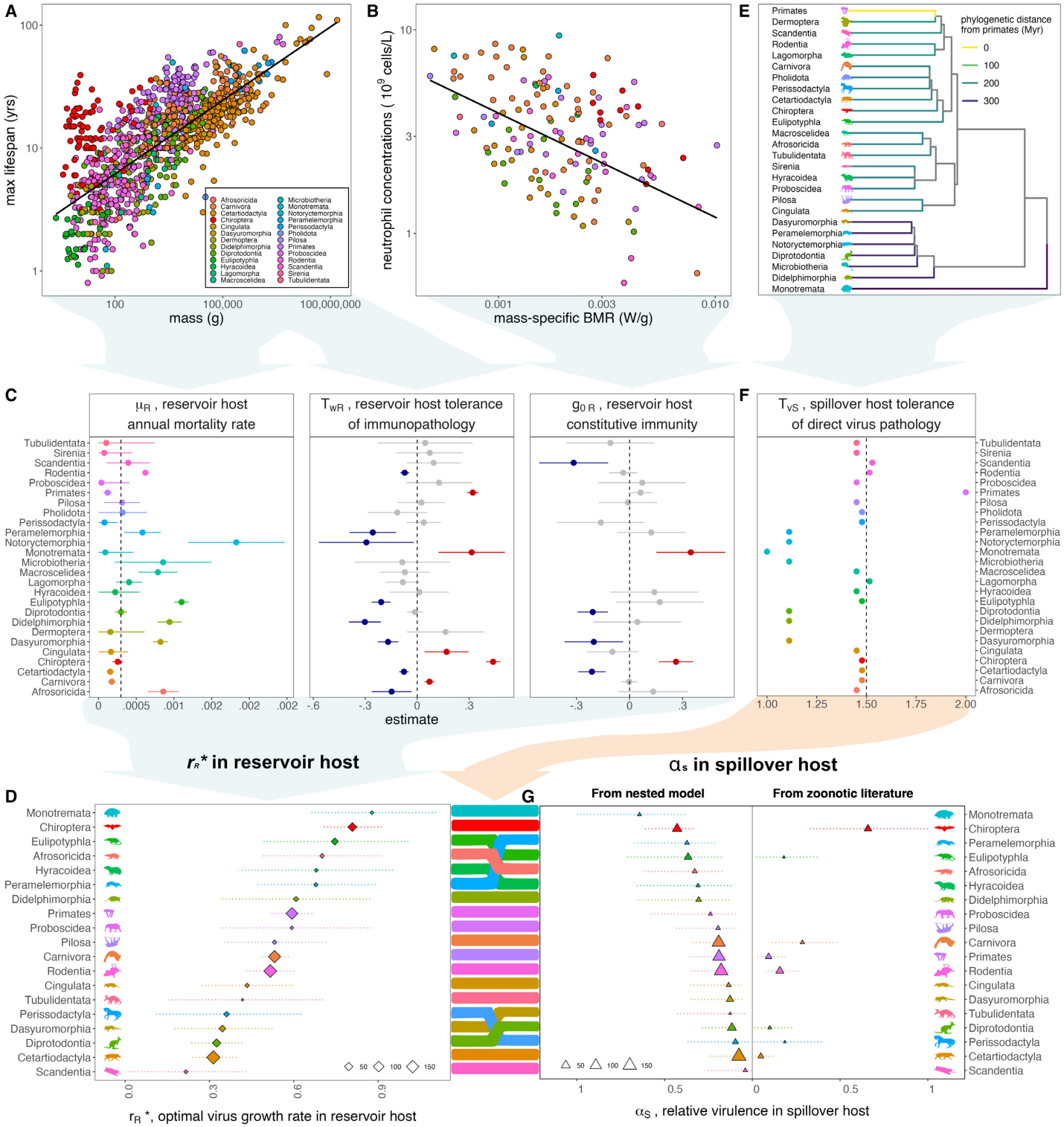

Fig 3. Reservoir host life history traits predict evolution of zoonotic virus virulence. (**A**) Variation in $\log_{10}$ maximum lifespan (y-axis, in years) with $\log_{10}$ adult body mass (x-axis, in grams) across mammals, with data derived from Jones and colleagues [54] and Healy and colleagues [55]. Points are colored by mammalian order, corresponding to legend. Black line depicts predictions of mammalian lifespan per body mass, summarized from fitted model (but excluding random effect of mammalian order), presented in S2 Table. (**B**) Baseline neutrophil concentrations (y-axis, in 10^9 cells/L) per mass-specific metabolic rate (x-axis, in W/g) across mammals, with data from Jones and colleagues [54] and Healy and colleagues [55] combined with neutrophil concentrations from Species360 [53]. Black line projects neutrophil concentration per mass-specific metabolic rate (excluding random effects of mammalian order), simplified from fitted model presented in S2 Table. (**C**)

Order-level parameters for nested modeling framework were derived from fitting of linear models and linear mixed models visualized here and presented in S4 Fig and S2 Table to data from (A) and (B). Average annual mortality rate (μ_R) was predicted from a linear regression of species-level annual mortality (the inverse of maximum lifespan), as described by a predictor variable of host order; tolerance of immunopathology (T_{wR}) was derived from the scaled effect of host order on the linear mixed effects regression of $\log_{10}$ maximum lifespan (in years) by $\log_{10}$ mass (in grams), incorporating a random effect of order. The magnitude of constitutive immunity (g_{0R}) was derived from the scaled effect of order on the regression of $\log_{10}$ neutrophil concentration per $\log_{10}$ body mass (in grams), combined with BMR (in W) (S4 Fig and S1 and S2 Tables). Panels shown here give numerical estimates for μ_R and order-level effects from fitted models that were scaled to numerical values for T_{wR} and g_{0R}, as presented in S4 Fig (S1 Table). Red and blue colors correspond to, respectively, significantly positive or negative order-level partial effects from these regressions. (**D**) Reservoir-host estimates for μ_R, T_{wR}, and g_{0R} were combined in our modeling framework to generate a prediction of optimal growth rate for a virus evolved in a host of each mammalian order (r_R^*). Here, point size corresponds to the average number of species-level data points used to generate each of the 3 variable parameters impacting r_R^*, as indicated in legend. (**E**) Phylogenetic distance from Primates (in millions of years, indicated by color) on a timescaled phylogeny, using data from TimeTree [56]. (**F**) An order-level estimate for the nested model parameter, T_{vS}, the spillover human host tolerance of pathology induced by a virus evolved in a different reservoir order, was estimated as the scaled inverse of the phylogenetic distance shown in (E) (S4 Fig and S1 Table). (**G**) Reservoir-host predictions of optimal virus growth rates (r_R^*) from (D) were combined with human spillover host estimates of tolerance for direct virus pathology (T_{vS}) from (F) in our nested modeling framework to generate a prediction of the relative spillover virulence (α_S) of a virus evolved in a given reservoir host order immediately following spillover into a secondary, human host. Here, the left panel visualizes predictions from our nested modeling framework, using order-specific parameters for μ_R, T_{wR}, g_{0R}, and T_{vS} (S1 Table). The right panel depicts relative human α_S estimates derived from case fatality rates and infection duration reported in the zoonotic literature [8]. For the left panel, point size corresponds to the average number of species-level data points used to generate each of the 4 variable parameters impacting α_S. For the right panel, point size indicates the total number of independent host–virus associations from which virulence estimates were determined. In (C), (D), and (G), 95% confidence intervals were computed by standard error; in (G) for the left panel, these reflect the upper and lower confidence intervals of the optimal virus growth rate in (D). See S1 Table for order-level values for r_R^*, μ_R, T_{wR}, g_{0R}, and T_{vS} and Table 1 for all other default parameters involved in calculation of α_S. Sensitivity analyses for zoonotic predictions are summarized in S5–S9 Figs and S3 Table. Data and code used to generate all figure panels are available in our publicly available GitHub repository (github.com/brooklabteam/spillover-virulence-v1.0.0; doi: 10.5281/zenodo.8136864).

https://doi.org/10.1371/journal.pbio.3002268.g003

hypothesis, we scale T_{wR} after order-level deviations in lifespan as predicted by body mass. To this end, we fit a linear mixed effect regression with a random effect of host order to the $\log_{10}$ relationship of lifespan (in years) as predicted by body size (in grams), again spanning data representing 26 diverse mammalian orders. From this, we identify 5 orders (Carnivora, Chiroptera, Cingulata, Monotremata, and Primates) with significantly longer lifespans than predicted by body size—which scale to enhanced estimates for T_{wR}. By contrast, we identify 8 orders (Afrosoricida, Cetartiodactyla, Dasyuromorphia, Didelphimorphia, Eulipotyphla, Notoryctemorphia, Peramelemorphia, and Rodentia) with significantly shorter lifespans than predicted by body size, which scale to lower value estimates for T_{wR} (Figs 3A, 3C, S4 and S1 and S2 Tables). Because the same data on host lifespan are included in both estimation of μ_R and T_{wR}, order-level estimates for T_{wR} largely mirror those for μ_R—such that longer-lived orders are modeled with low values for annual mortality rate and high values for tolerance to immunopathology (and vice versa). However, because mass is not factored into estimation of μ_R, these parameters diverge in select cases: for example, we estimate mid-range mortality rates for order Chiroptera, as compared with other mammals, but very high values for T_{wR} becase Chiropteran lifespans—though not remarkably long at face value—far exceed those predicted by body size. By contrast, we estimate low values for both μ_R and T_{wR} for order Cetartiodactyla, as hosts in this order are long-lived but less long-lived than predicted for body size.

Finally, we fit another linear mixed effect regression with a random effect of host order to the $\log_{10}$ relationship of baseline circulating neutrophil concentration (in 10^9 cells/L) as predicted by mass (in grams) and BMR (W); these data spanned only 19 mammalian orders (Fig 3B). From this, we identify a significant positive association between the orders Chiroptera and Monotremata and the response variable of baseline neutrophil concentration, indicating that species in these orders may have more enhanced constitutive immune responses than predicted by mass-specific BMR (Fig 3C). The orders Cetartiodactyla, Dasyuromorphia, Diprotodontia, and Scandentia, by contrast, show significant negative associations, representing lower baseline neutrophil concentrations than predicted per mass-specific BMR. We scale these order-level effects to correspondingly high and low estimates for g_{0R}, the within-host parameter representing the magnitude of reservoir-host constitutive immunity in our nested modeling framework (Figs 3B, 3C, S4 and S1 and S2 Tables).

From life history-derived estimates for μ_R, T_{wR}, and g_{0R}, we next generate a prediction of the optimal growth rate of a virus evolved in a reservoir host $\left(r_R^*\right)$ for each of 19 distinct mammalian orders for which we possess the full suite of proxy data for all 3 variable within-host parameters (Fig 3D). In keeping with results from our general model (Fig 2), we predict the evolution of high r_R^* viruses from reservoir orders exhibiting high μ_R, T_{wR}, and/or g_{0R}. Because our nested model expresses parameters in timesteps most relevant to viral dynamics (days), differences in mortality rates across mammalian orders—though substantial on multiyear timescales of the host—have limited influence on downstream predictions of differences in the evolution of virus growth rates. This result echoes prior observations from Fig 2, which showed reduced sensitivity of r_R^* to realistic variation in the magnitude of μ_R, as compared with other parameters. As a result, we ultimately recover the highest predicted optimal growth rates for viruses evolved in the orders Chiroptera and Monotremata, which exhibit both long lifespans per body size (corresponding to high estimates for T_{wR}) and high baseline neutrophil concentrations (corresponding to high estimates for g_{0R}). Data are particularly sparse, however, for order Monotremata, for which complete records are only available for 2 species (the platypus and the short-beaked echidna). As a result, predictions for this order should be interpreted with caution. More data, particularly for baseline neutrophil concentrations, will be needed to evaluate the extent to which these predictions hold across all 5 extant species in the Monotremata order. Additionally, we predict the evolution of the lowest growth rate viruses in reservoir hosts of the orders Scandentia, Cetartiodactyla, Diprotodontia, and Dasyuromorphia, all of which demonstrate significantly low estimates for the magnitudes of constitutive immunity and 2 of which (Cetartiodactyla, Dasyuromorphia) also demonstrate significantly low estimates for tolerance of immunopathology.

Estimating zoonotic virus virulence in spillover human hosts

After establishing optimal growth rates for viruses evolved in diverse reservoir host orders (r_R^*), we subsequently model the corresponding "spillover virulence" (α_S) of these viruses following emergence into a human host. Zoonotic spillovers are modeled as acute infections in the human, and virulence is calculated while varying only the growth rate of the spillover virus (r_R^*) and the human tolerance of direct virus pathology (T_{vS}) between viruses evolved in differing reservoir orders. We vary this last parameter, T_{vS}, to account for any differences in virus adaptation to reservoir host immune systems that are not already captured in estimation of reservoir host T_{wR} and g_{0R}. T_{vS} is thus computed as the inverse of the scaled time to MRCA for each mammalian reservoir host order from Primates (Figs 3E, S4 and S1 and S2 Tables), such that we estimate low human tolerance to viruses evolved in phylogenetically distant orders (e.g., monotreme and marsupial orders), and high human tolerance to viruses evolved in Primate and Primate-adjacent orders. In general, the modulating effects of T_{vS} do little to alter virulence rankings of zoonotic viruses from those predicted by raw growth rate (r_R^*) alone—with the highest spillover virulence predicted from viruses evolved in orders Monotremata and Chiroptera and the lowest spillover virulence predicted from viruses evolved in orders Cetartiodactyla and Scandentia (Fig 3D and 3G). Notably, modulating T_{vS} enhances predictions of spillover virulence for some marsupial clades (Peramelemorphia, Dasyuromorphia, Diprotodontia) relative to eutherian orders with similar predicted r_R^* values. This results in dampened predicted spillover virulence for the eutherian order Perissodactyla as compared with marsupial orders Dasyuromorphia and Diprotodontia, despite lower predicted r_R^* values for the latter 2 clades (Figs 3D, 3G, and S5). Similarly, this elevates spillover virulence predictions for Peramelemorphia above Eulipotyphla, Afrosoricida, and Hyrocoidea, despite higher predicted r_R^* in the 3 eutherian orders (Figs 3D, 3G, and S5).

Comparing predictions of spillover virulence by reservoir order with estimates from the literature

Since parameter magnitudes estimated from life history traits are largely relative in nature, we scale predictions of spillover virulence (α_S) by reservoir order in relative terms to compare with estimates gleaned from the zoonosis literature [8] (Figs 3G and S5–S9). For 8 reservoir orders (Chiroptera, Eulipotyphla, Primates, Carnivora, Rodentia, Diprotodontia, Perissodactyla, and Cetartiodactyla), we are able to fit a simple linear regression comparing the relative virulence of zoonoses derived from each order as reported from case fatality rates in the literature [4,8] versus those predicted by our nested modeling approach (S6 and S8 Figs and S3 Table). Our nested modeling framework recovers available case fatality rate data well, yielding an R^2 value of 0.57 in the corresponding regression of observed versus predicted values (S6 Fig and S3 Table). Critically, we successfully recover the key result from the zoonosis literature: bat-derived zoonoses yield higher rates of virus-induced mortality upon spillover to humans (α_S) than do viruses derived from all other eutherian mammals (Figs 3G and S5–S8). In general, high estimates for T_{wR}, μ_R, and g_{0R}, and low estimates for T_{vS} predict high spillover virulence to humans (α_S). Bats demonstrate uniquely long lifespans for their body sizes and uniquely enhanced constitutive immune responses [21] as compared with other taxa; when combined, as in our analysis, to represent high T_{wR} and high g_{0R}, these reservoir host traits elevate predicted r_R^* and α_S beyond all other eutherian orders (Fig 3D and 3G).

Evaluated against the data [4,8], our model overpredicts cross-order comparative virulence rankings for viruses evolved in order Eulipotyphla (Figs 3G and S6), largely as a result of our parameterization of high values for annual mortality rate (μ_R) and correspondingly low values for tolerance of immunopathology (T_{wR}) in this order. In addition, our model underpredicts virulence for Carnivora-derived viruses, based on within-host parameter estimates largely inverse to those recovered for Eulipotyphla (e.g., low μ_R and high T_{wR}). We are able to resolve this underprediction of Carnivora virulence when excluding rabies lyssavirus from data comparisons [4,8] (S8 Fig); though most rabies zoonoses are sourced from domestic dogs, lyssaviruses are Chiropteran by origin [63], and viral traits responsible for rabies' virulence may reflect its bat evolutionary history more than that of any intermediate carnivore host. Nonetheless, while excluding rabies from comparison improves recovery of literature-estimated relative virulence of Carnivora-derived viruses, it somewhat destabilizes predictions for other orders, such that the overall performance of the model is largely equivalent as to when comparing against all available data (S8 Fig; $R^2 = 0.57$).

In all cases, our model successfully reproduces estimates of significantly lower virulence incurred by zoonotic viruses evolved in Cetartiodactyla hosts as compared with all other orders considered [8]. While previous work suggested that low observed virulence for Cetartiodactylan zoonoses might result from overreporting of avirulent zoonoses in domestic livestock with frequent human contact [8], our analysis indicates that viral zoonoses emerging from Cetartiodactylan hosts may truly be less virulent to humans. Our mechanistic framework demonstrates that reduced tolerance of immunopathology (manifest as shorter lifespans than predicted by body size) and limited constitutive immune responses identified in Cetartiodactylan hosts may drive the evolution of low growth rate viruses that cause correspondingly benign infections following zoonotic emergence. Further research into the extent to which Cetartiodactylans are impacted by immunopathology, as well as the degree to which low reported baseline neutrophil concentrations accurately reflect their innate immunity, is needed to evaluate these predictions. Quantification of the natural growth rates of Cetartiodactylan-evolved viruses could offer one means of testing this modeling framework.

Sensitivity analyses demonstrate that, as previously observed in Fig 2, within-host parameters have unequal impacts on the resulting prediction of spillover virulence in our nested modeling framework (S9 Fig and S3 Table). Individually profiling T_{wR}, g_{0R}, and T_{vS} while holding all other parameters constant across host orders is insufficient to recover previously reported estimates of spillover virulence for zoonoses. Nonetheless profiling g_{0R}—and to a lesser extent T_{vS} or T_{wR}—while paired with order-specific estimates generated from life history data for the other 2 parameters greatly improves our recovery of spillover virulence as reported in the literature (yielding an R^2 value of 0.99 from the corresponding regression of observed versus predicted values; S9 Fig and S3 Table). These findings suggest that no single parameter in our nested modeling framework underpins observed variation in predicted spillover virulence across reservoir host orders; still, g_{0R}, the magnitude of constitutive immunity attributed to each reservoir order, appears to modulate these resulting differences to a greater extent than do T_{vS} and T_{wR}.

Discussion

Our work formalizes a mechanistic hypothesis into the biological processes that underpin cross-species patterns in the evolution of virus virulence—a major advance for efforts to evaluate zoonotic risk. Using a simple model of evolving virus in a reservoir host immune system, we successfully recapture patterns previously reported in the literature that document both the extreme virulence of viral zoonoses derived from bats and the surprising avirulence of viruses derived from Cetartiodactylan hosts [8]. Notably, our nested modeling approach produces rank-ordered predictions of spillover virulence recovered in the literature [8], which are distinct from those that would result from a scaled inversion of phylogenetic distance alone. Additionally, our mechanistic approach allows us to make powerful predictions about the virulence of potential future viral spillovers, using general life history traits across mammals, including from orders for which zoonoses have not yet been reported [8]. Our model indicates that we should anticipate the evolution of high growth rate viruses likely to cause virulence upon cross-species emergence from mammalian hosts with protracted lifespans for their body size (which we link to molecular mechanisms of immunopathological tolerance [49]), as well as from hosts with robust constitutive immune responses [36]. While both immunopathological tolerance and constitutive immunity should drive the evolution of high growth rate viruses (Fig 2), only tolerance will do so in the absence of reservoir host pathology, thus highlighting its importance in driving observed variation in the virulence of viral zoonoses. Notably, while tolerance reduces pathogen-induced mortality for a single host, tolerant host populations (with limited checks on virus transmission) may demonstrate high pathogen prevalence. If imperfectly tolerant hosts still experience some virus-induced pathology, high prevalence can consequently elevate total population-level mortality for infected hosts—a phenomenon known as the "tragedy of tolerance" [40,41]. Reports of virus-induced mortality in bats are rare [64], suggesting that bat virus tolerance is likely very effective.

Intriguingly, our independent evaluations of mammalian life history traits associated with enhanced longevity (which we model as a proxy for immunopathological tolerance) and robust constitutive immunity highlight several mammalian orders—chiefly Chiroptera and Monotremata—which show synergy in both features, offering support for ongoing efforts to elucidate links between antiaging molecular pathways and antiviral immunity [59,64]. Further bolstering these hypotheses, we demonstrate the inverse synergy in order Cetartiodactyla, which exhibits shorter than predicted lifespans per body size but significantly reduced constitutive immune responses as compared with other mammals. Though exciting, our predictions should nonetheless be regarded with considerable caution, as taxon-specific insights resulting

from our modeling framework are limited by a dearth of comparative data. For example, we characterize host tolerance of immunopathology based on deviations in lifespan as predicted for body size because more directly representative measures of, for example, mammalian antioxidant capacity, are not universally available. In addition, we model variation in reservoir host immunology almost exclusively based on variation in baseline neutrophil concentrations across mammalian orders, while holding constant many basic immunological parameters that almost certainly vary across taxa. Though crude, baseline neutrophil data nonetheless produce an estimate of enhanced constitutive immune responses for order Chiroptera, which is robustly supported by independent molecular work describing constitutive interferon expression in bat cells across multiple species [21,65,66].

All told, this analysis highlights a critical need for compilation of a more complete comparative immunological database that would enable quantification of the many additional within-host parameters (e.g., leukocyte activation rate, virus consumption rate, leukocyte mortality rate, and host tolerance of direct virus pathology) represented in our model. Our relative success in recapturing broad patterns in spillover virulence, despite data constraints, suggests that improvements in parameter estimation will almost certainly yield gains in our nuanced understanding of the process of cross-species virus emergence. For example, we model host tolerance of direct virus pathology as proportional to phylogenetic distance between reservoir and spillover host, but this term will likely also be modulated by virus tropism—presenting yet another mechanism by which viral adaptation to reservoir hosts could enhance spillover virulence. Indeed, coronavirus tropism is thought to be localized largely in the gastrointestinal tract for bat hosts [67,68]: In our modeling framework, higher tolerance of direct virus pathology in this tissue should promote the evolution of higher growth rate viruses in bats, which are likely to cause virulence upon infection of more vulnerable tissues, such as the respiratory tract, in spillover hosts.

By summarizing within-host traits across mammalian orders, we generalize substantial within-clade diversity that likely also contributes to heterogeneous patterns in available data. Bats alone make up more than 1,400 species and account for some 20% of mammalian diversity [69]. Only a subset of bats are long-lived [70], and the magnitude of constitutive immunity is known to vary across bat species [21,36,44], suggesting considerable variation in the parameters μ_R, T_{wR}, and g_{0R}, which we here model universally across the entire Chiropteran order. Thus, we can expect considerable variation in the evolution of virulence for viruses evolved in diverse species within a given order—which we largely disregard here. As more data becomes available, our modeling approach could be fine-tuned to make more specific, species-level predictions of highly virulent disease risk.

Our analysis does not consider the probability of cross species viral emergence, or the potential for onward transmission of a spilled-over virus in a human host—both of which have been shown to correlate inversely with phylogenetic distance across mammals [4,8,9]. Indeed, in keeping with trade-off theory, onward transmission of viruses following spillover is more commonly associated with low virulence infections [6,8,71,72], suggesting that reservoir orders highlighted here as potential sources for high virulence pathogens are not necessarily the same orders likely to source future pandemics. Nonetheless, the possibility for virus adaptation to gain transmission advantages in human hosts following spillover—as witnessed for Ebola [73] and SARS-CoV-2 [74]—should not be ignored.

Currently, our work emphasizes the uniqueness of bats as flying mammals and, in consequence, as long-lived, tolerant reservoirs for highly virulent viral zoonoses. For the first time, we formalize a mechanism for the evolution of bat-derived viruses that demonstrate significant pathology upon spillover to non-bat, particularly human, hosts. In providing a theoretical framework to explain this phenomenon, we generate a series of testable questions and

hypotheses for future comparative immunological studies, to be carried out at *in vitro* and *in vivo* scales. Empirical work should aim to measure rates of immune cell activation, growth, and mortality across diverse mammalian orders and determine whether natural virus growth rates are truly higher when evolved in bat hosts. Additional studies should test whether anti-inflammatory mechanisms in bat cells of different tissues are equally effective at mitigating virus-induced pathology and immunopathology and whether comparative taxonomic predictions of virus tolerance, resistance, and virulence evolution apply to non-viral pathogens, too. In light of the emergence of SARS-CoV-2, the field of bat molecular biology has echoed the call for mechanistic understanding of bat immunology [75], and the NIH has responded [76], soliciting research on the development of tools needed to test the predictions outlined here. We offer a bottom-up mechanistic framework enabling the prediction of emerging virus virulence from the basic immunological and life-history traits of zoonotic hosts.

Methods

Evolutionary framework

Population-level dynamics. To evaluate the selective pressures that drive the evolution of cross-species virus virulence, we first derive an equation for an optimal virus growth rate expressed in within-host parameters specific to the life history of the reservoir host. To this end, and in keeping with classic examples of viral maintenance in reservoir populations [77–83], we first model the dynamics of a persistent infection (I_1) in a hypothetical reservoir host, allowing for the introduction of a rare mutant virus strain which generates distinct infections in that same host (I_2) (see S1 File for more detailed methodology and derivations):

$$\frac{dS}{dt} = N(b_R - q_R N) - \beta_{r_{1R}} S I_1 - \beta_{r_{2R}} S I_2 - \mu_R S \tag{1a}$$

$$\frac{dI_1}{dt} = \beta_{r_{1R}} S I_1 - \mu_R I_1 - \alpha_{r_{1R}} I_1 \tag{1b}$$

$$\frac{dI_2}{dt} = \beta_{r_{2R}} S I_2 - \mu_R I_2 - \alpha_{r_{2R}} I_2. \tag{1c}$$

Here, N corresponds to the total host population and S to all hosts susceptible to infection, such that $N = S + I_1 + I_2$. We assume that hosts are born at rate b_R and die of natural death at rate μ_R, where $b_R > \mu_R$. We further assume that all hosts are born susceptible and that population density is regulated via a crowding term (q_R) applied to the birth rate. The subscript "$_R$" on the birth, death, and crowding terms emphasizes that these rates are specific to the reservoir host. Because we aim to model the evolution of rates that link to within-host dynamics for the reservoir host, we further represent transmission and virulence as functions of the virus causing the infection (respectively, β_{r_R} and α_{r_R}), where r_R denotes the intrinsic virus growth rate and is represented distinctly for both the endemic (r_{1R}) and mutant (r_{2R}) virus strains.

With the use of model (1), we perform an evolutionary invasion analysis (see S1 File) and conclude that the virus should evolve to maximize the ratio of transmission over infection duration. We refer to this ratio as the invasion fitness:

$$\frac{\beta_{r_R}}{\mu_R + \alpha_{r_R}}. \tag{2}$$

Within-host dynamics. Next, to evaluate the within-host selective conditions underpinning the evolution of the virus growth rate (r_R), we express the between-host parameters of transmission (β_{r_R}) and virulence (α_{r_R}) in within-host terms, using a nested modeling approach. To this end, we establish a simple within-host model representing the dynamics of infection within each I_1 and I_2 host as outlined above. We follow Alizon and Baalen (2005) [45] to adapt a class of Lotka–Volterra predator–prey-like within-host models (reviewed in [84]), to overcome some constraints of basic predator–prey models of the immune system, chiefly (i) by allowing leukocytes to circulate in the absence of infection; and (ii) by scaling leukocyte growth with virion density, independent of direct leukocyte-virion contact [45,85,86]. This results in the following model, which demonstrates interactions between the virus population (V_R) and the leukocyte population (L_R) within each infected reservoir host:

$$\frac{dV_R}{dt} = r_R V_R - c_R V_R L_R \tag{3a}$$

$$\frac{dL_R}{dt} = g_{0R} + g_R r_R V_R - m_R L_R. \tag{3b}$$

Here, r_R corresponds to the intrinsic virus growth rate, c_R corresponds to the attack efficacy of the immune system upon contact with the virus, and g_R signifies the recruitment rate of immune cells scaled to the virus growth rate. The parameter, g_{0R}, describes the constitutive, baseline leukocyte recruitment in the absence of infection, and m_R gives the natural leukocyte death rate, all in the reservoir host.

Building from above, we express rates of population-level transmission and virulence known to depend on within-host dynamics ($\beta_{r_{1R}/r_{2R}}$ and $\alpha_{r_{1R}/r_{2R}}$) in terms of their within-host components, assuming that within-host dynamics are fast relative to host population-level dynamics and, therefore, converge to the endemic equilibrium (i.e., $m_R r_R > c_R g_{0R}$).

In line with previous work, we assume transmission to be a linear function of viral load [45], which we represent as:

$$\beta_{r_R} = \zeta V_R^*. \tag{4}$$

Where ζ corresponds to a scaling term equating viral load to transmission. We additionally assume that:

$$\alpha_{r_R} = \frac{v r_R V_R^*}{T_{vR}} + \frac{w g_R r_R V_R^*}{T_{wR}}, \tag{5}$$

by which infection-induced host mortality ("virulence") is modeled to result from both virus-induced pathology (a function of the intrinsic virulence of the parasite, v, multiplied by the parasite growth rate $r_R V_R^*$) and immunopathology—which we model as proportional to the leukocyte growth rate (g_R) multiplied by the virus growth rate ($r_R V_R^*$) multiplied by the parasite's intrinsic propensity for host immune antagonism (w). The terms T_{vR} and T_{wR} correspond to host tolerance of virus-induced pathology and immunopathology, respectively, under assumptions of "constant" tolerance, by which both virus pathology and immunopathology are reduced by a constant proportion across the course of infection. For constant tolerance, we assume that $T_{vR} > 1$ and $T_{wR} > 1$. See S1 File for detailed derivations under assumptions of "complete" tolerance, whereby virus pathology and immunopathology are completely eliminated up to a threshold value, beyond which pathology scales proportionally with virus and immune cell growth.

Now, we rewrite the equations for transmission (4) and virulence (5) in purely within-host terms:

$$\beta_{r_R} = \frac{\zeta(m_R r_R - c_R g_{0R})}{c_R g_R r_R} \tag{6}$$

$$\alpha_{r_R} = \frac{v(m_R r_R - c_R g_{0R})}{c_R g_R T_{vR}} + \frac{w(m_R r_R - c_R g_{0R})}{c_R T_{wR}}. \tag{7}$$

Using these within-host expressions, we then recompute the expression for invasion fitness (2) in within host terms and determine the optimal intrinsic virus growth rate, which is an evolutionarily stable strategy (ESS) (see S1 File):

$$r_R^* = \frac{c_R g_{0R}}{m_R} + \frac{\sqrt{c_R^2 m_R^2 g_R g_{0R} \mu_R T_{vR} T_{wR}(v T_{wR} + g_R w T_{vR})}}{m_R^2 (v T_{wR} + g_R w T_{vR})}. \tag{8}$$

In Fig 2, we explore the sensitivity of r_R^*, and the corresponding reservoir host population-level transmission ($\beta_{r_R}^*$) and virulence ($\alpha_{r_R}^*$) at that growth rate, across varied values for its within-host component parameters.

Cross-species dynamics. We next derive an expression to explore the consequences of spillover of a virus evolved to its optimal growth rate in a reservoir host population—which we term r_R^*—following cross-species emergence into the human population. Contrary to its established persistent infection in the reservoir host, we assume that such a virus will produce an acute infection in the spillover host. To model the dynamics of this acute spillover, we borrow from Gilchrist and Sasaki [47], who developed a within-host parasite–leukocyte model in which an immortal leukocyte successfully eradicates the parasite population to near-zero. We modify their acute model to be more comparable to our chronic infection model ((3a)/(3b)) and to reflect our differing notation for within-host dynamics.

$$\frac{dV_S}{d\tau} = r_R^* V_S - c_S V_S L_S. \tag{9a}$$

$$\frac{dL_S}{d\tau} = r_R^* g_S V_S. \tag{9b}$$

Here, r_R^* represents the reservoir-evolved virus growth rate, but all other terms reflect within-host conditions of the spillover host: V_S and L_S correspond, respectively, to the spillover host virus and leukocyte populations, c_S is the virus consumption rate upon contact with leukocytes in the spillover host, and g_S is the growth rate of the spillover host leukocyte population in response to virus. We express the model in units of τ, which we assume to be short in comparison to the t time units of dynamics in the reservoir host population. Rather than solving for virus and leukocyte populations at equilibrium (as in the reservoir host population), we follow Gilchrist and Sasaki [47] to instead derive an expression for the virus population at the peak of infection ($V_{S_{max}}$), where we anticipate maximum pathology for the spillover host. We then extend this prior work to generate an expression for the average viral load ($V_{S_{avg}}$) in the spillover host across the timecourse of acute infection, which we can use in comparisons of spillover host virulence with reported case fatality rates for zoonoses in the literature.

If we divide Eq (9a) by Eq (9b), we derive a simple time-independent relationship between virus and leukocyte density:

$$\frac{dV_S}{dL_S} = \frac{1}{g_S}\left(1 - \frac{c_S L_S}{r_R^*}\right). \tag{10}$$

If we then let $L_S(0) = 1$, $V_S(0) = 1$, assuming that both virus and leukocyte populations will be small at $\tau = 0$, we can integrate (10) to establish the following relationship between virus and leukocyte:

$$V_S = \frac{1}{g_S}L_S - \frac{c_S}{2r_R^* g_S}(L_S)^2 + 1 - \frac{1}{g_S} + \frac{c_S}{2r_S^* g_S}. \tag{11}$$

Notice that the above (11) is simply a quadratic equation (see (12) below):

$$V_S(L_S) = -\frac{c_S}{2r_R^* g_S}(L_S)^2 + \frac{1}{g_S}L_S + \left(1 - \frac{1}{g_S} + \frac{c_S}{2r_S^* g_S}\right). \tag{12}$$

Now, we can take the derivative of Eq (12) to formulate an expression for V_{Smax}, the maximum viral load, which should precede the end of acute infection and the point of host recovery at the maximum duration of infection:

$$V_{Smax} = \frac{r_R^*}{g_S c_S} - \frac{r_R^*}{2g_S c_S} + 1 - \frac{1}{g_S} + \frac{c_S}{2r_R^* g_S}. \tag{13}$$

Then, extending previous work [47], we calculate the average viral load by taking the integral of Eq (12) from $V_S(0)$ to V_{Smax} and dividing by the duration of that interval. From this exercise, we express the average value of Eq (12) as:

$$V_{Savg} = \frac{r_R^*\sqrt{c_S^2 + 2r_R^*(g_S - 1)c + \left(r_R^*\right)^2} + \left(r_R^*\right)^2 + 4r_R^*(g-1)c + 2c_S^2}{6c_S g_S r_R^*}. \tag{14}$$

Now, with this established expression for V_{Savg}, we adapt Eq (7) to reflect the acute within-host dynamics of "spillover virulence," which we model (as before) as a combination of mortality induced from direct virus pathology and from immunopathology. As in the reservoir host system, we also model the mitigating impact of tolerance on the 2 mechanisms of virulence:

$$\alpha_S = V_{Savg}\left(\frac{r_R^* v}{T_{vS}} + \frac{g_S w r_R^*}{T_{wS}}\right). \tag{15}$$

This yields the above expression for "spillover virulence." Here, the growth rate of the virus is expressed at its evolutionary optimum evolved in the reservoir host (r_R^*), and the virus's intrinsic virulence (v) and propensity to elicit an inflammatory immune response (w) remained unchanged from one host to the next. Inspired by findings in the literature that report higher virulence in cross-species infections between hosts separated by larger phylogenetic distances [8–12], we model spillover host tolerance of virus-induced pathology (T_{vS}) as a decreasing function of increasing phylogenetic distance between the reservoir and secondary host. All other immune-related parameters assume characteristics of the spillover host: g_S is the spillover host's leukocyte growth rate, and T_{wS} corresponds to the spillover host's tolerance of immunopathology.

Order-specific estimates for optimal virus growth rates evolved in reservoir hosts

Next, we develop estimates for the optimal virus growth rate (r_R^*) expected to evolve across a suite of diverse mammalian reservoir orders. Because within-host immunological data needed to quantify within-host parameters underpinning the expression for r_R^* are largely lacking, we proxy a few key within-host parameters from well-described allometric relationships for mammalian life history data. As such, we here focus on 3 key parameters for which data could be gleaned from the literature: the reservoir host mortality rate (μ_R), the reservoir host tolerance of immunopathology (T_{wR}), and the magnitude of reservoir host constitutive immunity (g_{0R}).

To generate order-level summary terms for μ_R we fit a simple linear regression to the response variable of the inverse of maximum lifespan (in days) with a single categorical predictor of host order, using data from Jones and colleagues [54] and Healy and colleagues [55] that span 26 mammalian orders and 1,060 individual species (Fig 3A). This first model thus takes the form:

$$Y_{ij} = \alpha_0 + \sum_{j=1}^{k-1} \beta_j \delta_{ij} + \varepsilon_{ij}, \quad (16)$$

where Y_{ij} corresponds to natural mortality rate observations for i species belonging to j orders; α_0 is the overall intercept; k indicates the total number of available orders (here, 26); β_j is an order-specific slope; δ_{ij} indicates observations of i species grouped into j orders; and ε_{ij} is a normally distributed error term corresponding to species i within order j. We estimate μ_R by simply generating predictions from this fitted model across all 26 mammalian orders represented in our dataset (Fig 3C and S2 Table).

We next use the same dataset of 1,060 species grouped into 26 mammalian orders to generate order-level estimates for the reservoir host tolerance of immunopathology (T_{wR}). Here, we fit a linear mixed effects regression to the $\log_{10}$ relationship of lifespan (in years) as predicted by body mass (in grams). This second model takes the form:

$$Y_{ij} = \alpha_0 + \beta_1 X_1 + u_{0j} + \varepsilon_{ij}, \quad (17)$$

where Y_{ij} corresponds to the $\log_{10}$ value of record of maximum lifespan (in years) for i species belonging to j orders; α_0 is the overall intercept; β_1 indicates the slope of the fixed predictor of $\log_{10}$ mass (in grams), here represented as X_1; u_{0j} is the order-specific random intercept; and ε_{ij} is a normally distributed error term corresponding to species i within order j. To estimate T_{wR}, we extract the relative partial effects of mammalian order on maximum lifespan per body size, and then rescale these effects between 1 and 2 for assumptions of constant tolerance and between 0 and 1 for assumptions of complete tolerance (S1 and S2 Tables). We justify this approach based on literature that highlights links between antiaging molecular pathways that promote longevity and those that mitigate immunopathology [11,44,57–61].

Finally, to generate order-level summary terms for the magnitude of constitutive immunity (g_0), we fit another linear mixed effects regression to the relationship between the predictor variables of $\log_{10}$ mass (in g) and BMR (in W) and the response variable of $\log_{10}$ baseline neutrophil concentration (in 10^9 cells/L), which offers an approximation of a mammal's constitutive innate immune response. BMR data for this model are derived from Jones and colleagues [54] and Healy and colleagues [55], while neutrophil concentrations were obtained from zoo animal data presented in the Species360 database [53]; prior work using this database has demonstrated scaling relationships between body size and neutrophil concentrations across mammals [52]. Paired neutrophil and BMR data were limited to just 19 mammalian orders and 144

species. Our model also includes a random effect of host order, resulting in the following form:

$$Y_{ij} = \alpha_0 + \beta_1 X_1 + \beta_2 X_2 + u_{0j} + \varepsilon_{ij}, \quad (18)$$

where Y_{ij} corresponds to the $\log_{10}$ baseline neutrophil concentrations (in 10^9 cells/L) for i species belonging to j orders; α_0 is the overall intercept; β_1 indicates the slope of the fixed predictor of $\log_{10}$ mass (in grams), here represented as X_1; β_2 indicates the slope of the fixed predictor of BMR (in W), here represented as X_2; u_{0j} is the order-specific random intercept; and ε_{ij} is a normally distributed error term corresponding to species i within order j. Using a similar approach as that employed above for T_{wR}, we estimate g_0 by extracting the relative partial effects of mammalian order on neutrophil concentration per mass-specific BMR, then rescale these effects between 0 and 1. Because we estimate significantly positive partial effects between the orders Chiroptera and Monotremata and baseline neutrophil concentration (Fig 3C), this generates correspondingly high estimates of g_{0R} for these two orders (S4 Fig and S1 Table).

Using these order-level summary terms for μ_R, T_{wR}, and g_{0R}, we then generate an order-level prediction for r_R^* across all mammalian host orders, following Eq (8) (Fig 3D). All other parameters (c_R, g_R, m_R, w, v, and T_{vR}) are held constant across all taxa at values listed in Table 1.

Estimating zoonotic virus virulence in spillover human hosts

Once we have constructed an order-level prediction for r_R^*, we explore the effects of these reservoir-evolved viruses upon spillover to humans, following Eq (15). As when computing virulence for the reservoir host population, we hold immunological parameters,c_S, g_S, and m_S constant in humans (at the same values listed above) due to a lack of informative data to the contrary. Then, to generate an order-level estimate for virus virulence incurred on humans (α_S), we combine our order-level predictions for r_R^* with order-specific values for T_{vS}, the human tolerance of an animal-derived virus, which we scale such that viruses derived from more closely related orders to Primates are more easily tolerated in humans. Specifically, we represent T_{vS} as the scaled inverse of the cophenetic phylogenetic distance of each mammalian order from Primates. No summarizing is needed for T_{vS} because, following Mollentze and Streicker [10], we use a composite timescaled reservoir phylogeny derived from the TimeTree database [56], which produces a single mean divergence date for all clades. Thus, all species within a given mammalian order are assigned identical times to MRCA with the order Primates. To convert cophenetic phylogenetic distance into reasonable values for T_{vS}, we divide all order-level values for this distance by the largest observed (to generate a fraction), then subtract that fraction from 2 for assumptions of constant tolerance (yielding T_{vS} estimates ranging from 1 to 2) and from 1 for assumptions of complete tolerance (yielding T_{vS} estimates ranging from 0 to 1).

We then combine reservoir host order-level predictions for r_R^* with these estimates for human tolerance of virus pathology (T_{vS}) to generate predictions of the expected spillover virulence of viral zoonoses emerging from the 19 mammalian orders for which we possess complete data across the 4 variable parameters (μ_R, T_{wR}, g_{0R}, and T_{vS}). We scale these α_S estimates —and their 95% predicted confidence intervals—in relative terms (from 0 to 1) to compare with estimates from the literature.

Comparing predictions of spillover virulence by reservoir order with estimates from the literature

To compare estimates of spillover virulence generated from our nested modeling approach (α_S) with estimates from the literature, we follow Day (2002) [87] to convert case fatality rates of viral zoonoses in spillover human hosts (CFR_S) reported in the literature [8] to empirical

estimates of α_S for each mammalian order, using data on the duration of human infection (D_{IS}) for each viral zoonosis. For this purpose, we collected data on D_{IS} by searching the primary literature; raw data for infection durations and associated references are reported in our publicly available GitHub repository (github.com/brooklabteam/spillover-virulence-v1.0.0; doi: 10.5281/zenodo.8136864). Briefly, Day (2002) [13] notes that the equation for case fatality rate in the spillover host (CFR_S) takes the form:

$$CFR_S = \frac{\alpha_S}{\alpha_S + \sigma_S}, \tag{19}$$

where σ_S corresponds to the recovery rate from the spilled-over virus in the human host. We also note that the total duration of infection, D_{IS}, is given by:

$$D_{IS} = \frac{1}{\alpha_S + \sigma_S}. \tag{20}$$

Therefore, we translated human case fatality rates of viral zoonoses (CFR_S) into estimates of spillover virulence (α_S) using the following equation:

$$\alpha_S = \frac{CFR_S}{D_{IS}}. \tag{21}$$

To obtain a composite order-level prediction for α_S from D_{IS} and CFR_S as reported in [8], we adopt the best-fit generalized additive model (GAM) [88] used by the authors in [8] to summarize CFR_S by order and, here, apply it to α_S estimates converted from CFR_S reported in the literature (S2 Table). This best-fit GAM estimates the response variable of spillover virulence (α_S) from corresponding predictor variables of reservoir host order, virus family, virus species publication count (a measure of research effort), spillover type (via bridge host versus direct), and vector-borne disease status (yes or no). Following [8], we summarize α_S at the order-level from the fitted GAM, excluding the effects of viral family, to yield a literature-derived value for α_S across disparate mammalian orders, against which to compare predictions from our nested modeling approach. Because the majority of the within-host parameters underpinning α_S predictions in our nested modeling approach (μ_R, T_{wR}, g_{0R}, and T_{vS}) are quantified only in a relative fashion, we were unable to compare direct magnitudes of virulence (e.g., in terms of host death per unit time). To account for this, we rescale α_S estimates from both our nested modeling approach and from the empirical literature from 0 to 1 and compare the relative rank of virulence by mammalian order instead. We predict α_S for 19 discrete mammalian orders, though data from the literature are available for only 8 orders against which to compare.

Finally, because bats are the most likely ancestral hosts of all lyssaviruses [63], and it may be more appropriate to class carnivores as "bridge hosts" for rabies, rather than reservoirs (as the authors discuss in Guth and colleagues (2022) [8]), we recompute literature-derived estimates of relative α_S by fitting the same GAMs (S2 Table) to a version of the dataset excluding all entries for rabies lyssavirus. We rescale these new estimates of spillover virulence between 0 and 1 and compare them again to predictions from our nested modeling approach.

To quantitatively evaluate the extent to which our nested model accurately recaptures estimates of relative spillover virulence (α_S) recovered from the literature, we fit a simple linear regression to the relationship between observed and predicted virulence across the 8 mammalian orders for which we possess comparative data (S6 and S8 Figs and S3 Table). We then determine the sensitivity of our predictions for α_S across reservoir orders to changes in the parameters we estimated from the literature. Because reservoir host natural mortality rate (μ_R) has minimal influence on optimal virus growth rates (r_R^*)—and because we assume mortality

data to be the most likely to be accurately reported in the literature—we focus this sensitivity analysis on the extent to which variation in estimation of reservoir host tolerance of immunopathology (T_{wR}), reservoir host magnitude of constitutive immunity (g_{0R}), and spillover host tolerance of reservoir-derived virus pathology (T_{vS}) impacts the resulting prediction for spillover virulence (α_S) (S9 Fig and S3 Table). To this end, we undertook 2 different analyses: first, we replaced order-specific values of T_{wR}, g_{0R}, and T_{vS} with constant values across all orders and profiled each of these 3 parameters in turn across a range of reasonable values; our aim here was to determine whether perturbation of a single parameter could replicate α_S estimates from the literature. Because this single parameter modulation was largely unsuccessful in recapturing order-specific differences in α_S, we next individually profiled T_{wR}, g_{0R}, and T_{vS} in turn while paired with life history-derived, order-specific values for the other 2 parameters, as presented in the main text (S9 Fig and S3 Table). To quantify the impact of this profiling on the accuracy with which we estimated spillover virulence across orders, we refit linear regressions of observed versus predicted spillover virulence using both parameter profiling approaches (S9 Fig and S3 Table).

Supporting information

S1 Fig. Pairwise invasibility plots demonstrate optimal viral growth rate, under low and high tolerance conditions. Invading growth rates (r_{R2}) will displace resident growth rates (r_{R1}) at values indicated by the shaded regions. Reservoir host tolerance of immunopathology (T_{wR}) and tolerance of direct virus pathology (T_{vR}) are both modeled as low in left column (0.5 and 10 for row 1 and 2, respectively) and high in right column (0.97 and 100 for row 1 and 2), assuming a complete (row 1) or a constant form (row 2). For this visualization, r_{R1} and r_{R2} span from 3.18 to 3.5. All other parameters involved in computation of r_R^* (see S1 File equations [25,26]) were fixed at values listed in Table 1 (main text). Data and code used to generate all figure panels are available in our publicly available GitHub repository (github.com/brooklabteam/spillover-virulence-v1.0.0; doi: 10.5281/zenodo.8136864).
(PNG)

S2 Fig. Optimal virus growth rates—and subsequent spillover virulence—vary across reservoir host immunological and life history parameters. Figure replicates Fig 2 (main text) under assumptions of complete tolerance. Rows (top-down) indicate the evolutionarily optimal within-host virus growth rate (r_R^*) and the corresponding transmission rate ($\beta^*_{r_R}$), and virus-induced mortality rate ($\alpha^*_{r_R}$) for a reservoir host infected with a virus at r_R^*. The bottom row then demonstrates the resulting virulence (α_S) of a reservoir-optimized virus evolved to r_R^* upon nascent spillover to a novel, secondary host. Columns demonstrate the dependency of these outcomes on variable reservoir host parameters: background mortality rate (μ_R), extent of constitutive immunity (g_{0R}), leukocyte activation rate upon viral contact (g_R), virus consumption rate by leukocytes (c_R), leukocyte mortality rate (m_R). Darker colored lines depict outcomes at higher values for reservoir host tolerance of virus pathology (T_{vR}, red) or immunopathology (T_{wR}, blue), assuming no tolerance of the opposing type. Heat maps demonstrate how T_{vR} and T_{wR} interact to produce each outcome. Outcome ranges differ between lineplots (y-axes) and heat maps (scale bars). Parameter values are listed in Table 1 (main text). Data and code used to generate all figure panels are available in our publicly available GitHub repository (github.com/brooklabteam/spillover-virulence-v1.0.0; doi: 10.5281/zenodo.8136864).
(PNG)

S3 Fig. Spillover host tolerance of direct virus pathology and immunopathology modulate resulting virulence of spilled-over viruses. Virulence of spilled-over virus (α_S) across a range

of values for 2 mechanisms of tolerance in the spillover host: tolerance of direct virus pathology (T_{vS}, left column) and tolerance of immunopathology (T_{wS}, right column). Results are expressed under assumptions of constant tolerance (top panels) and complete tolerance (bottom panels). In main text results, T_{wS} is held constant for all predictions of spillover virulence but T_{vS} is varied proportionally to the inverse time to MRCA between reservoir and spillover host. Data and code used to generate all figure panels are available in our publicly available GitHub repository (github.com/brooklabteam/spillover-virulence-v1.0.0; doi: 10.5281/zenodo.8136864).
(PNG)

S4 Fig. Parameter estimates for life history traits across mammalian orders. Model parameter estimates for (A) reservoir-host background mortality (μ_R), (B) tolerance of immunopathology (T_{wR}) (left y-axis: constant tolerance assumptions; right y-axis: complete tolerance assumptions), (C) magnitude of constitutive immunity (g_{0R}), and (D) magnitude of human tolerance of virus pathology for a virus evolved in a disparate mammalian reservoir (T_{vS}). Estimates are derived from (A) linear model predictions of maximum lifespan at the order level, (B) the scaled effect of order on a linear mixed model prediction of lifespan per body size, (C) the scaled effect of order on a linear mixed model prediction of neutrophil concentration for mass-specific BMR, and (D) the magnitude of human tolerance of virus pathology for a virus evolved in a disparate mammalian reservoir (T_{vS}), corresponding to data presented in Fig 3E (main text). Default parameter values involved in the estimation process are summarized in Table 1 (main text), and estimated parameters and corresponding 95% confidence intervals by standard error are presented in S1 Table. See main text Methods and our open-source GitHub repository for a detailed walk-through of the parameter estimation process. Data and code used to generate all figure panels are available in our publicly available GitHub repository (github.com/brooklabteam/spillover-virulence-v1.0.0; doi: 10.5281/zenodo.8136864).
(PNG)

S5 Fig. Optimal virus growth rates (r_R^*) and subsequent spillover virulence (α_S) for viruses evolved in diverse mammalian reservoirs. Figure replicates Fig 3D and 3G from the main text, here under assumptions of complete tolerance. Panel (A) depicts optimal r_R^* across 19 mammalian orders, for which we were able to estimate order-level specific values for the 3 within-host reservoir parameters which we varied in our analysis (μ_R, T_{wR}, and g_{0R}; visualized in S4 Fig), while panel (B) depicts the resulting estimation of relative spillover virulence (α_S), which also relies on order-specific values for the spillover host tolerance of direct virus pathology (T_{vS}). Taxa in panels (A) and (B) are arranged in descending order from highest to lowest predicted values for, respectively r_R^* and α_S. This order varies slightly from panel (A) to (B), as highlighted by alluvial flows and discussed in the main text. See S1 Table for order-level values for r_R^*, μ_R, T_{wR}, g_{0R}, and T_{vS} and Table 1 (main text) for all other parameters involved in calculation of r_R^* and α_S. Data and code used to generate all figure panels are available in our publicly available GitHub repository (github.com/brooklabteam/spillover-virulence-v1.0.0; doi: 10.5281/zenodo.8136864).
(PNG)

S6 Fig. Comparison of human spillover virulence (α_S) as observed in the literature vs. predicted from nested modeling framework. Figure plots observed vs. predicted spillover virulence for 8 orders from Fig 3G (main text) for which case fatality rates from corresponding zoonoses are reported in the literature [8]. Panel (A) compares nested modeling predictions under assumptions of constant tolerance with those from the literature, while panel (B) does the same under assumptions for complete tolerance. In both cases, a fitted linear regression

and corresponding R^2 value is shown as a quantitative evaluation of model fit to the data. Dashed lines give the residual of each data point from the regression line. Data and code used to generate all figure panels are available in our publicly available GitHub repository (github.com/brooklabteam/spillover-virulence-v1.0.0; doi: 10.5281/zenodo.8136864).
(PNG)

S7 Fig. Comparison of relative human spillover virulence (α_S) predictions for zoonoses from nested life history model with estimates from the literature, excluding rabies. Figure replicates Fig 3G (main text), respectively, under assumptions of (A) constant and (B) complete tolerance but excluding rabies lyssavirus from the zoonotic data (right-half of panels). Rank-order predictions of virulence are more consistent with order Carnivora further down in the rankings. As in Fig 3G, order-specific parameter values for r_R^*, μ_R, T_{wR}, g_{0R}, and T_{vS} are listed in S1 Table; all other parameters involved in calculation of α_S are listed in Table 1 (main text). Data and code used to generate all figure panels are available in our publicly available GitHub repository (github.com/brooklabteam/spillover-virulence-v1.0.0; doi: 10.5281/zenodo.8136864).
(PNG)

S8 Fig. Comparison of human spillover virulence (α_S) as observed in the literature (excluding rabies) vs. predicted from nested modeling framework. Plot recapitulates S6 Fig exactly, but comparisons are drawn from case fatality rates reported in the literature but excluding rabies lyssavirus, which is often classed as a Carnivora-derived virus, though its evolutionary origins are found in bats. Removal of rabies improves estimates of virulence for Carnivora-derived zoonoses as compared with the complete dataset, but resulting linear regression offers no better fit to the entire dataset than previously shown in S6 Fig. Data and code used to generate all figure panels are available in our publicly available GitHub repository (github.com/brooklabteam/spillover-virulence-v1.0.0; doi: 10.5281/zenodo.8136864).
(PNG)

S9 Fig. Sensitivity analysis of individual parameter influence on nested model fit to observed data. Figure replicates S6 Fig in part with observed spillover virulence (α_S) from case fatality rates reported in the literature [8] depicted on the x-axis and predictions from nested modeling framework on the y-axis. In all panels, circles correspond to nested modeling predictions of spillover virulence using parameter values recovered from regression analysis of publicly available life history data as presented in the main text, replicating points from S6 Fig. Projections from nested modeling approach assuming constant tolerance are shown in the top panels and complete tolerance in the bottom. In lieu of life history-derived parameter values, squares show α_S estimates from nested model using constant, universal values across all orders for all parameters excepting the parameter profiled in the corresponding column (T_{wR}, T_{vS}, or g_{0R}). When not profiled, T_{wR} = 1.5 (constant) and 0.5 (complete); T_{vS} = 1.5 (constant) and 0.5 (complete); and g_{0R} = 0.5 for simulations resulting in square points. Finally, triangles give α_S estimates from nested model approach using parameters generated by profiling the parameter in the corresponding column (T_{wR}, T_{vS}, or g_{0R}), while pairing it with values recovered using regression analysis the literature for other variable parameters (S1 Table). Lines and corresponding R^2 values signify the fit of a simple linear regression of observed vs. predicted α_S across all mammalian orders, where predicted values are generated from nested modeling approach using: linear regression analysis of life history data for T_{wR}, T_{vS}, and g_{0R} (solid line, red, same as reported in the main text); profiling T_{wR}, T_{vS}, or g_{0R} while holding constant all other parameters across orders (thin dashed line); and profiling T_{wR}, T_{vS}, or g_{0R} while using linear regression estimates from life history data for parameters not being profiled (thick

dashed line). Data and code used to generate all figure panels are available in our publicly available GitHub repository (github.com/brooklabteam/spillover-virulence-v1.0.0; doi: 10.5281/zenodo.8136864).
(PNG)

S1 Table. Order-specific parameter values for within-host nested model.
(PDF)

S2 Table. Model summary outputs for within-host parameter estimation.
(PDF)

S3 Table. Sensitivity analysis and comparison of influence of individual parameter estimates on overall fit of nested model to data.
(PDF)

S1 File. Supplementary Information Text.
(PDF)

Acknowledgments

The authors thank the Boots Lab at UC Berkeley and the Brook lab at the University of Chicago for helpful comments on this manuscript. This work was completed in part with resources provided by the University of Chicago's Research Computing Center.

Author Contributions

Conceptualization: Cara E. Brook, Mike Boots.

Data curation: Cara E. Brook, Sarah Guth.

Formal analysis: Cara E. Brook, Carly Rozins.

Funding acquisition: Cara E. Brook.

Investigation: Cara E. Brook.

Methodology: Cara E. Brook, Carly Rozins, Sarah Guth.

Project administration: Cara E. Brook.

Supervision: Mike Boots.

Validation: Cara E. Brook.

Visualization: Cara E. Brook.

Writing – original draft: Cara E. Brook.

Writing – review & editing: Carly Rozins, Sarah Guth, Mike Boots.

References

1. Bonneaud C, Longdon B. Emerging pathogen evolution. EMBO Rep. 2020; 21:e51374.
2. André JB, Hochberg ME. Virulence evolution in emerging infectious diseases. Evolution. 2005; 59 (7):1406. PMID: 16153027
3. Bolker BM, Nanda A, Shah D. Transient virulence of emerging pathogens. J R Soc Interface. 2010; 7 (46):811–822. https://doi.org/10.1098/rsif.2009.0384 PMID: 19864267
4. Guth S, Visher E, Boots M, Brook CE. Host phylogenetic distance drives trends in virus virulence and transmissibility across the animal—human interface. Philos Trans R Soc B. 2019; 374 (1782):20190296. https://doi.org/10.1098/rstb.2019.0296 PMID: 31401961

5. Farrell MJ, Davies TJ. Disease mortality in domesticated animals is predicted by host evolutionary relationships. Proc Natl Acad Sci U S A. 2019; 116(16):7911–7915. https://doi.org/10.1073/pnas.1817323116 PMID: 30926660

6. Mollentze N, Streicker DG, Murcia PR, Hampson K, Biek R. Virulence mismatches in index hosts shape the outcomes of cross-species transmission. Proc Natl Acad Sci U S A [Internet]. 2020. Available from: http://www.ncbi.nlm.nih.gov/pubmed/33122433. https://doi.org/10.1073/pnas.2006778117 PMID: 33122433

7. Longdon B, Hadfield JD, Day JP, Smith SCL, McGonigle JE, Cogni R, et al. The causes and consequences of changes in virulence following pathogen host shifts. Schneider DS, editor. PLoS Pathog. 2015 Mar 16; 11(3):e1004728. https://doi.org/10.1371/journal.ppat.1004728 PMID: 25774803

8. Guth S, Mollentze N, Renault K, Streicker DG, Visher E, Boots M, et al. Bats host the most virulent—but not the most dangerous—zoonotic viruses. Proc Natl Acad Sci U S A. 2022 Apr 5; 119(14): e2113628119. https://doi.org/10.1073/pnas.2113628119 PMID: 35349342

9. Olival KJ, Hosseini PR, Zambrana-Torrelio C, Ross N, Bogich TL, Daszak P. Host and viral traits predict zoonotic spillover from mammals. Nature [Internet]. 2017. Available from: http://www.nature.com/doifinder/10.1038/nature22975.

10. Mollentze N, Streicker DG. Viral zoonotic risk is homogenous among taxonomic orders of mammalian and avian reservoir hosts. Proc Natl Acad Sci U S A. 2020;1–8. https://doi.org/10.1073/pnas.1919176117 PMID: 32284401

11. Irving AT, Ahn M, Goh G, Anderson DE, Wang LF. Lessons from the host defences of bats, a unique viral reservoir. Nature. 2021; 589(842):363–370.

12. Schountz T, Baker ML, Butler J, Munster V. Immunological control of viral infections in bats and the emergence of viruses highly pathogenic to humans. Front Immunol. 2017; 8:1098. https://doi.org/10.3389/fimmu.2017.01098 PMID: 28959255

13. Boots M. Fight or learn to live with the consequences. Trends Ecol Evol. 2008; 23(5):245–248.

14. Råberg L, Sim D, Read AF. Disentangling genetic variation for resistance and tolerance to infectious diseases in animals. Science. 2007; 318(5851):812–814. https://doi.org/10.1126/science.1148526 PMID: 17975068

15. Råberg L, Graham AL, Read AF. Decomposing health: tolerance and resistance to parasites in animals. Philos Trans R Soc Lond B Biol Sci. 2009; 364(1513):37–49. https://doi.org/10.1098/rstb.2008.0184 PMID: 18926971

16. Mougari S, Gonzalez C, Reynard O, Horvat B. Fruit bats as natural reservoir of highly pathogenic henipaviruses: balance between antiviral defense and viral tolerance. Curr Opin Virol. 2022 Jun; 54:101228.

17. Ng M, Ndungo E, Kaczmarek M, Herbert AS, Binger T, James R, et al. NPC1 contributes to species-specific patterns of Ebola virus infection in bats. Elife. 2015; 4:e11785.

18. Starr TN, Zepeda SK, Walls AC, Greaney AJ, Alkhovsky S, Veesler D, et al. ACE2 binding is an ancestral and evolvable trait of sarbecoviruses. Nature. 2022 Mar 31; 603(7903):913–918. https://doi.org/10.1038/s41586-022-04464-z PMID: 35114688

19. Letko M, Miazgowicz K, McMinn R, Seifert SN, Sola I, Enjuanes L, et al. Adaptive evolution of MERS-CoV to species variation in DPP4. Cell Rep. 2018; 24(7):1730–1737. https://doi.org/10.1016/j.celrep.2018.07.045 PMID: 30110630

20. Letko M, Marzi A, Munster V. Functional assessment of cell entry and receptor usage for SARS-CoV-2 and other lineage B betacoronaviruses. Nat Microbiol. 2020; 5(4):562–569. https://doi.org/10.1038/s41564-020-0688-y PMID: 32094589

21. Zhou P, Tachedjian M, Wynne JW, Boyd V, Cui J, Smith I, et al. Contraction of the type I IFN locus and unusual constitutive expression of IFN-α in bats. Proc Natl Acad Sci U S A. 2016 Mar 8; 113(10):2696–2701.

22. Laing ED, Sterling SL, Weir DL, Beauregard CR, Smith IL, Larsen SE, et al. Enhanced autophagy contributes to reduced viral infection in black flying fox cells. Viruses. 2019; 11(3). https://doi.org/10.3390/v11030260 PMID: 30875748

23. Chionh YT, Cui J, Koh J, Mendenhall IH, Ng JHJ, Low D, et al. High basal heat-shock protein expression in bats confers resistance to cellular heat/oxidative stress. Cell Stress Chaperones. 2019; 24(4):835–849. https://doi.org/10.1007/s12192-019-01013-y PMID: 31230214

24. Jebb D, Huang Z, Pippel M, Hughes GM, Lavrichenko K, Devanna P, et al. Six reference-quality genomes reveal evolution of bat adaptations. Nature. 2020 Jul 23; 583(7817):578–584. https://doi.org/10.1038/s41586-020-2486-3 PMID: 32699395

25. Hayward JA, Tachedjian M, Cui J, Cheng AZ, Johnson A, Baker ML, et al. Differential evolution of antiretroviral restriction factors in Pteropid bats as revealed by APOBEC3 gene complexity. Teeling E,

editor. Mol Biol Evol. 2018 Jul 1; 35(7):1626–1637. https://doi.org/10.1093/molbev/msy048 PMID: 29617834

26. O'Shea TJ, Cryan PM, Cunningham AA, Fooks AR, Hayman DTS, Luis AD, et al. Bat flight and zoonotic viruses. Emerg Infect Dis. 2014 May; 20(5):741–745. https://doi.org/10.3201/eid2005.130539 PMID: 24750692
27. Thomas BYSP, Suthers RA. The physiology and energetics of bat flight. J Exp Biol. 1972; 57:317–335.
28. Speakman J, Thomas D. Physiological ecology and energetics of bats. In: Kunz T, Fenton M, editors. Bat ecology. Chicago: University of Chicago Press; 2003. p. 430–90.
29. Zhang G, Cowled C, Shi Z, Huang Z, Bishop-Lilly KA, Fang X, et al. Comparative analysis of bat genomes provides insight into the evolution of flight and immunity. Science. 2013 Jan 25; 339 (6118):456–460. https://doi.org/10.1126/science.1230835 PMID: 23258410
30. Santillan DM, Lama T, Guti Y, Brown A, Zhao H, Rossiter S, et al. Large-scale genome sampling reveals unique immunity and metabolic adaptations in bats. Mol Ecol. 2021.
31. Ahn M, Cui J, Irving AT, Wang LF. Unique loss of the PYHIN gene family in bats amongst mammals: Implications for inflammasome sensing. Sci Rep. 2016; 6(August 2015):21722. https://doi.org/10.1038/srep21722 PMID: 26906452
32. Ahn M, Anderson DE, Zhang Q, Tan CW, Lim BL, Luko K, et al. Dampened NLRP3-mediated inflammation in bats and implications for a special viral reservoir host. Nat Microbiol [Internet] 2019; 4(May). Available from: http://dx.doi.org/10.1038/s41564-019-0371-3 https://doi.org/10.1038/s41564-019-0371-3 PMID: 30804542
33. Xie J, Li Y, Shen X, Xie J, Li Y, Shen X, et al. Dampened STING-dependent interferon activation in bats. Cell Host Microbe. 2018; 23:1–5.
34. Goh G, Ahn M, Zhu F, Lee L, Luo D, Irving AT. Complementary regulation of caspase-1 and IL-1 β reveals additional mechanisms of dampened inflammation in bats. Proc Natl Acad Sci U S A. 2020.
35. Austad SN, Fischer KE. Mammalian aging, metabolism, and ecology: evidence from the bats and marsupials. J Gerontol. 1991 Mar; 46(2):B47–B53. https://doi.org/10.1093/geronj/46.2.b47 PMID: 1997563
36. Brook CE, Boots M, Chandran K, Dobson AP, Drosten C, Graham AL, et al. Accelerated viral dynamics in bat cell lines, with implications for zoonotic emergence. Elife. 2020; 9:e48401. https://doi.org/10.7554/eLife.48401 PMID: 32011232
37. Ebert D, Bull JJ. Challenging the trade-off model for the evolution of virulence: is virulence management feasible? Trends Microbiol. 2003 Jan; 11(1):15–20. https://doi.org/10.1016/s0966-842x(02)00003-3 PMID: 12526850
38. Alizon S, Hurford A, Mideo N, Van Baalen M. Virulence evolution and the trade-off hypothesis: History, current state of affairs and the future. J Evol Biol. 2009; 22(2):245–259. https://doi.org/10.1111/j.1420-9101.2008.01658.x PMID: 19196383
39. Anderson RM, May RM. Coevolution of hosts and parasites. Parasitology. 1982; 85:411–426. https://doi.org/10.1017/s0031182000055360 PMID: 6755367
40. Miller MR, White A, Boots M. The evolution of parasites in response to tolerance in their hosts: The good, the bad, and apparent commensalism. Evolution. 2006; 60(5):945. PMID: 16817535
41. Best A, White A, Boots M. The coevolutionary implications of host tolerance. Evolution. 2014 May; 68 (5):1426–1435. https://doi.org/10.1111/evo.12368 PMID: 24475902
42. Randolph HE, Barreiro LB. Holy Immune Tolerance, Batman! Immunity. 2018; 48(6):1074–1076. https://doi.org/10.1016/j.immuni.2018.05.016 PMID: 29924972
43. Hayman DTS. Bat tolerance to viral infections. Nat Microbiol. 2019; 4(5):728–729. https://doi.org/10.1038/s41564-019-0430-9 PMID: 31015739
44. Pavlovich SS, Lovett SP, Koroleva G, Guito JC, Arnold CE, Nagle ER, et al. The Egyptian Rousette genome reveals unexpected features of bat antiviral immunity. Cell. 2018; 173:1–13.
45. Alizon S, van Baalen M. Emergence of a convex trade-off between transmission and virulence. Am Nat. 2005; 165(1537–5323 (Electronic)):E155–E167. https://doi.org/10.1086/430053 PMID: 15937740
46. Geritz SAH, Kisdi É, Meszéna G, Metz JAJ. Evolutionarily singular strategies and the adaptive growth and branching of the evolutionary tree. Evol Ecol. 1998; 12(1):35–57.
47. Gilchrist MA, Sasaki A. Modeling host–parasite coevolution: A nested approach based on mechanistic models. J Theor Biol. 2002; 218:289–308. https://doi.org/10.1006/jtbi.2002.3076 PMID: 12381431
48. Boots M, Donnelly R, White A. Optimal immune defence in the light of variation in lifespan. Parasite Immunol. 2013; 35(11):331–338. https://doi.org/10.1111/pim.12055 PMID: 23869870

49. Brown J, West G, Enquist B. Scaling in biology: Patterns and processes, causes and consequences. In: Scaling in biology. Oxford University Press; 2000. p. 87–112.

50. Brown JH, Gillooly JF, Allen AP, Savage VM, West GB. Towards a metabolic theory of ecology. Ecology. 2004; 85(7):1771–1789.

51. West GB, Woodruff WH, Brown JH. Allometric scaling of metabolic rate from molecules and mitochondria to cells and mammals. Proc Natl Acad Sci U S A. 2002; 99(SUPPL. 1):2473–2478. https://doi.org/10.1073/pnas.012579799 PMID: 11875197

52. Downs CJ, Dochtermann NA, Ball R, Klasing KC, Martin LB. The effects of body mass on immune cell concentrations of mammals. Am Nat. 2020; 195(1):107–114. https://doi.org/10.1086/706235 PMID: 31868541

53. Species360 Zoological Information Management System (ZIMS) [Internet]. [cited 2022 Aug 25]. https://zims.species360.org/.

54. Jones KE, Bielby J, Cardillo M, Fritz SA, O'Dell J, Orme CDL, et al. PanTHERIA: a species-level database of life history, ecology, and geography of extant and recently extinct mammals. Ecology. 2009; 90 (9):2648–2648.

55. Healy K, Guillerme T, Finlay S, Kane A, Kelly BA, Mcclean D, et al. Ecology and mode-of-life explain lifespan variation in birds and mammals. Proc R Soc B. 2014. https://doi.org/10.1098/rspb.2014.0298 PMID: 24741018

56. Kumar S, Stecher G, Suleski M, Hedges SB. TimeTree: a resource for timelines, timetrees, and divergence times. Mol Biol Evol. 2017; 34:1812–1819. https://doi.org/10.1093/molbev/msx116 PMID: 28387841

57. Wilkinson GS, Adams DM, Haghani A, Lu AT, Zoller J, Breeze CE, et al. DNA methylation predicts age and provides insight into exceptional longevity of bats. Nat Commun [Internet]. 2021; 12(1). Available from: http://dx.doi.org/10.1038/s41467-021-21900-2.

58. Dhinaut J, Balourdet A, Teixeira M, Chogne M, Moret Y. A dietary carotenoid reduces immunopathology and enhances longevity through an immune depressive effect in an insect model. Sci Rep. 2017 Dec 1; 7(1).

59. Caruso C, Lio D, Cavallone L. Aging, longevity, inflammation, and cancer. Ann N Y Acad Sci. 2004; 1028:1–13. https://doi.org/10.1196/annals.1322.001 PMID: 15915584

60. Fabian DK, Garschall K, Klepsatel P, Santos-Matos G, Sucena É, Kapun M, et al. Evolution of longevity improves immunity in *Drosophila*. Evol Lett. 2018 Dec; 2(6):567–579.

61. Kolora SRR, Owens GL, Vazquez JM, Stubbs A, Chatla K, Jainese C, et al. Origins and evolution of extreme life span in Pacific Ocean rockfishes. Science. 2021 Nov 12; 374(6569):842–847. https://doi.org/10.1126/science.abg5332 PMID: 34762458

62. Speakman JR. Body size, energy metabolism and lifespan. J Exp Biol. 2005; 208:1717–1730. https://doi.org/10.1242/jeb.01556 PMID: 15855403

63. Rupprecht CE, Turmelle A, Kuzmin IV. A perspective on lyssavirus emergence and perpetuation. Curr Opin Virol. 2016; 1(6):662–670.

64. Brook CE, Dobson AP. Bats as 'special' reservoirs for emerging zoonotic pathogens. Trends Microbiol. 2015; 23(3):172–180. https://doi.org/10.1016/j.tim.2014.12.004 PMID: 25572882

65. Shaw AE, Hughes J, Gu Q, Behdenna A, Singer JB, Dennis T, et al. Fundamental properties of the mammalian innate immune system revealed by multispecies comparison of type I interferon responses. Malik H, editor. PLoS Biol. 2017 Dec 18; 15(12):e2004086. https://doi.org/10.1371/journal.pbio.2004086 PMID: 29253856

66. Clayton E, Munir M. Fundamental characteristics of bat interferon systems. Front Cell Infect Microbiol. 2020 Dec 11; 10:527921. https://doi.org/10.3389/fcimb.2020.527921 PMID: 33363045

67. Widagdo W, Begeman L, Schipper D, Run PRV, Cunningham AA, Kley N, et al. Tissue distribution of the MERS-coronavirus receptor in bats. Sci Rep. 2017 Dec; 7(1):1193. https://doi.org/10.1038/s41598-017-01290-6 PMID: 28446791

68. Ruiz-Aravena M, McKee C, Gamble A, Lunn T, Morris A, Snedden CE, et al. Ecology, evolution and spillover of coronaviruses from bats. Nat Rev Microbiol. 2021. https://doi.org/10.1038/s41579-021-00652-2 PMID: 34799704

69. Simmons N, Cirranello A. Bat species of the world: A taxonomic and geographic database [Internet]. 2020 [cited 2020 Jul 11]. https://batnames.org/.

70. Wilkinson GS, Adams DM. Recurrent evolution of extreme longevity in bats. Biol Lett. 2019; 15:20180860. https://doi.org/10.1098/rsbl.2018.0860 PMID: 30966896

71. Geoghegan JL, Senior AM, Di F, Holmes EC. Virological factors that increase the transmissibility of emerging human viruses. Proc Natl Acad Sci U S A. 2016; 113(15):4170–4175. https://doi.org/10.1073/pnas.1521582113 PMID: 27001840

72. Longdon B, Hadfield JD, Webster CL, Obbard DJ, Jiggins FM. Host phylogeny determines viral persistence and replication in novel hosts. PLoS Pathog. 2011; 7(9). https://doi.org/10.1371/journal.ppat.1002260 PMID: 21966271

73. Urbanowicz RA, Mcclure CP, Sakuntabhai A, Sall AA, Kobinger G, Muller MA, et al. Human adaptation of Ebola virus during the West African Outbreak. Cell. 2016; 167:1079–1087. https://doi.org/10.1016/j.cell.2016.10.013 PMID: 27814505

74. Plante JA, Liu Y, Liu J, Xia H, Johnson BA, Lokugamage KG, et al. Spike mutation D614G alters SARS-CoV-2 fitness. Nature [Internet]. 2020;(September). Available from: http://dx.doi.org/10.1038/s41586-020-2895-3.

75. Wang LF, Gamage AM, Chan WOY. Decoding bat immunity: the need for a coordinated research approach. Nat Rev Immunol. 2021; 21(5):269–271. https://doi.org/10.1038/s41577-021-00523-0 PMID: 33649605

76. National Institutes of Health. Research on Bat Immunology [Internet]. https://grants.nih.gov/grants/guide/pa-files/PAR-21-184.html.

77. Viana M, Mancy R, Biek R, Cleaveland S, Cross PC, Lloyd-Smith JO, et al. Assembling evidence for identifying reservoirs of infection. Trends Ecol Evol. 2014 May; 29(5):270–279. https://doi.org/10.1016/j.tree.2014.03.002 PMID: 24726345

78. Hampson K, Haydon DT. Persistent pathogens and wildlife reservoirs. Science. 2021; 374(6563):35–36. https://doi.org/10.1126/science.abl8885 PMID: 34591640

79. Haydon DT, Cleaveland S, Taylor LH, Laurenson MK. Identifying reservoirs of infection: A conceptual and practical challenge. Emerg Infect Dis. 2002 Dec; 8(12):1468–1473. https://doi.org/10.3201/eid0812.010317 PMID: 12498665

80. Jolles A, Gorsich E, Gubbins S, Beechler B, Buss P, Juleff N, et al. Endemic persistence of a highly contagious pathogen: Foot-and-mouth disease in its wildlife host. Science. 2021 Oct; 374(6563):104–109. https://doi.org/10.1126/science.abd2475 PMID: 34591637

81. Plowright RK, Peel AJ, Streicker DG, Gilbert A, McCallum H, Wood J, et al. Transmission or within-host dynamics driving pulses of zoonotic viruses in reservoir-host populations. PLoS Negl Trop Dis. 2016; 10(8):e0004796. https://doi.org/10.1371/journal.pntd.0004796 PMID: 27489944

82. Schountz T, Prescott J, Cogswell AC, Lauren O, Mirowsky-Garcia K, Galvez AP, et al. Regulatory T cell-like responses in deer mice persistently infected with Sin Nombre virus. Proc Natl Acad Sci U S A. 2007; 104(39):15496–15501. https://doi.org/10.1073/pnas.0707454104 PMID: 17875986

83. Schountz T, Prescott J. Hantavirus immunology of rodent reservoirs: Current status and future directions. Viruses. 2014; 6:1317–1335. https://doi.org/10.3390/v6031317 PMID: 24638205

84. Alizon S, van Baalen M. Acute or Chronic? Within-host models with immune dynamics, infection outcome, and parasite evolution. Am Nat. 2008; 172(6):E244–E256. https://doi.org/10.1086/592404 PMID: 18999939

85. Alizon S, van Baalen M. Multiple infections, immune dynamics, and the evolution of virulence. Am Nat. 2008; 172(4):E150–E168. https://doi.org/10.1086/590958 PMID: 18702601

86. Fenton A, Lello J, Bonsall MB. Pathogen responses to host immunity: The impact of time delays and memory on the evolution of virulence. Proc Biol Sci. 2006; 273(1597):2083–2090. https://doi.org/10.1098/rspb.2006.3552 PMID: 16846917

87. Day T. On the evolution of virulence and the relationship between various measures of mortality. Proc R Soc B. 2002; 269:1317–1323. https://doi.org/10.1098/rspb.2002.2021 PMID: 12079653

88. Wood SN. mgcv: GAMs and Generalized Ridge Regression for R. R News. 2001; 1/2:20–24.